Modeling and Control of Flapping Wing Micro Aerial Vehicles

by

Shiba Biswal

A Thesis Presented in Partial Fulfillment
of the Requirements for the Degree
Master of Science

Approved April 2015 by the
Graduate Supervisory Committee:

Armando Rodriguez, Co-Chair
Marc Mignolet, Co-Chair
Spring Berman

ARIZONA STATE UNIVERSITY

May 2015

ABSTRACT

Interest in Micro Aerial Vehicle (MAV) research has surged over the past decade. MAVs offer new capabilities for intelligence gathering, reconnaissance, site mapping, communications, search and rescue, etc. This thesis discusses key modeling and control aspects of flapping wing MAVs in hover. A three degree of freedom nonlinear model is used to describe the flapping wing vehicle. Averaging theory is used to obtain a nonlinear average model. The equilibrium of this model is then analyzed. A linear model is then obtained to describe the vehicle near hover. LQR is used to as the main control system design methodology. It is used, together with a nonlinear parameter optimization algorithm, to design a family multivariable control system for the MAV. Critical performance trade-offs are illuminated. Properties at both the plant output and input are examined. Very specific rules of thumb are given for control system design. The conservatism of the rules are also discussed. Issues addressed include

1. What should the control system bandwidth be vis–vis the flapping frequency (so that averaging the nonlinear system is valid)?

2. When is first order averaging sufficient? When is higher order averaging necessary?

3. When can wing mass be neglected and when does wing mass become critical to model? This includes how and when the rules given can be tightened; i.e. made less conservative.

To my parents

ACKNOWLEDGEMENTS

I am grateful to Dr. Rodriguez, my advisor, for believing in me, and letting me work in this exciting research area. His enthusiasm towards every project and his immense experience in this field, was a constant motivation, if I could ever have a fraction of his expertise, I would consider myself very lucky.

This thesis would not have been possible without Dr. Mignolet. I am forever indebted, for he patiently guided me through my mistakes. Over the 2 years, he has become a mentor and supported me through some tough times. Words can not do justice to the gratitude I feel for him.

I would also like to thank my first controls professor and my committee member Dr. Spring Berman who has significantly influenced my academic experience at ASU. She is very supportive and a gem of a person.

I am very grateful to Dr. Armbruster at ASU for helping me with the concepts of averaging. I am grateful to Dr. Taha (University of California, Irvine) and Dr. Sun (Beihang University, China) for taking out time from their busy schedules and answering my questions.

Special thanks to my best friend Karthik, who has been a big support, motivation and confidante.

I would like to thank all my friends here with whom I have had wonderful 3 years, they have all been part of my ups and downs, Monica, Aniket, Roshan, Krithika, Deepthi, Kenan, Ricky, Deepak, Karan, Justin, Kaustav and Heather. I would like to acknowledge all my friends in India.

Last but not the least, my parents and my sister, their unconditional love and support means the world to me and without their support, this MS journey would not have been possible.

TABLE OF CONTENTS

CHAPTER Page

LIST OF FIGURES

Figure Page

Chapter 1

INTRODUCTION

The miracles of nature are seen in the diversity of species. In this constantly changing world where we are pushing the envelope of technological advancement, humans have always derived inspiration from this diversity. There is a constant strive to replicate the wonders of nature, that evolution has so well optimized. One such diversity seen is in animal flight. While the research in unmanned aerial vehicles has been surging, research in flapping wing micro aerial vehicles (MAV), although not new, has received relatively moderate amount of attention. The motivation for these flapping wing MAV comes from insect flight, which has always captivated biologists and aerodynamicists. It is a case of curiosity that such tiny beings perform extremely complex flight maneuvers with very low energy. In fact, up until 1930's insect flight was deemed impossible! Insect flight show tremendous variations, for e.g. a butterfly flaps at about 5 Hz, where as a tiny ceratopogonid flaps at around 1000 Hz! Flight of every insect changes with shape of the wing, size of the body, wing beat pattern and so on. A common house fly, although annoying is quite a marvelous flier, anybody who has tried swatting it, can vouch for its maneuverability. In this thesis, we have tried answering the challenges involved in modeling, designing and controlling of flight of flapping wing micro aerial vehicles, that mimic insect flight.

1.1 Literature Review

The research presented here is built on diverse array of work. Some of them that have contributed significantly towards the completion of this thesis have been listed in this section. Zbikowski (2005) is a good read on how flies are able to control their

flight. It discusses some of the morphological features they possess that enable their superior flight. Taha *et al.* (2012), Orlowski and Girard (2012), Sun (2014), provide an extensive literature review of the research so far, in the field of flapping wing micro aerial vehicles. The first two works compare methods and approaches used by various groups of researchers, for aerodynamics modeling, system dynamics modeling and flight control methodologies, whereas the latter gives a summary of most of the research done so far.

Most of the research in MAVs have concentrated on the hover state. There are several reasons for treating hover as a benchmark problem, as listed by Ellington (1999). Equations for power are simple, forward flight would add to the complexity, hovering flight would provide a practical test bed for MAVs, pendulum stability (body hanging below wing bases) minimizes control problems, lift coefficients only decline with increasing speed and lastly the power requirement of hovering would also be adequate for forward flight. Thus, if a MAV that hovers can be built, it will also be able to support its weight and power the wings over virtually the entire speed range.

The first aspect that we discuss is the aerodynamic modeling. A comprehensive review of work done in insect flight aerodynamic modeling is given in Ansari *et al.* (2006a). Insect flight aerodynamics have been studied for years. Before the advent of CFD, researchers relied on direct measurement of wing kinematics and forces from flapping flight for analysis. The seminal work of Ellington (1984c) uses quasi steady state aerodynamics for analysis. Kinematics for hover of many insects were studied in this six part series paper. New theory for lift and power mechanisms were introduced. Forward flight in Bumblebees was studied later by Dudley and Ellington (1990a). Traditionally, it was believed that flapping wings created lift the same way an aircraft's wing did, but the secret to the lift production being 2-3 times the body weight was attributed to leading edge vortices formed on the wings (Ellington *et al.*

(1996)). Further breakthrough in the analysis of insect flight took place in the mid 1990s, when a scaled robotic flapper was built to study relationship between wing kinematics and force production by Dickinson *et al.* (1999). Existence of 3 main distinct phases of the flapping cycle namely delayed stall, rotational circulation and wake capture, all resulting from non steady nature of flapping, were shown. The drag and lift coefficients reported in this paper have been widely used by the flapping wing MAV community. Based on their findings, they revised the existing quasi steady aerodynamic model (Sane and Dickinson (2002)). A review of the aerodynamic phenomena have been provided by Sane (2003) and Wang (2005). Later Dickinson and group conducted the same experiment on the mechanical wings but with wings given a finite velocity, to analyze effect of forward flight on the aerodynamics (Dickson and Dickinson (2004)). CFD greatly helped in corroborating the experimental results. One such notable work is that of Ramamurti and Sandberg (2002). Zhang and Sun (2010) and Wu *et al.* (2009) solve the Navier Stokes equation coupled with rigid body dynamics. The two part paper of Ansari *et al.* (2006b,c) remains till date the most comprehensive aerodynamic model, they solve two novel coupled, non linear wake integral equations numerically.

Aerodynamics of the wings is decided by the wing kinematics. The reason insects are able to maneuver so well, is because they employ their wing degrees of freedom differentially. This means that each wing is able to rotate independently of the other, in all 3 axes. This gives great flexibility. To be able to map these kinematics to the body degrees of freedom, force analysis and the interplay/coupling of these kinematics has been studied by many. A point to note is that allowed kinematics is limited by the actuation power that is available. Actual wing kinematics for various hovering insects were recorded by Ellington (1984a) using high speed photography. The same author recorded Hawkmoth wing kinematics in both hover and forward flight in Will-

mott and Ellington (1997a). Bumblebees in forward flight were captured by Dudley and Ellington (1990a). Most of the studies concluded the relative importance of these wing kinematics for flight control, and these are namely, the stroke plane angle (the plane in which the wing stroke takes place, with respect to the longitudinal axis of the body), wing flapping parameters including the amplitude, offset and frequency and lastly the wing pitching angle magnitude in both upstroke and downstroke and timing of stroke reversal. The impact of changing some of these parameters on force production was experimentally determined in Sane and Dickinson (2001). The importance of asymmetric kinematics in forward flight was studied in Yu and Tong (2005). Analysis of few of these wingstroke kinematics from a controls perspective, for longitudinal flight is done by Humbert and Faruque (2011). The relative significance of few chosen parameters when the flight condition changes from hovering to forward flight is examined by Wu and Sun (2009). Berman and Wang (2007) use an optimization algorithm to find the kinematics that minimizes the energy in out, at hover. Power consideration in deciding MAV wing kinematics is an important aspect but not much literature is available on this. Hedrick and Daniel (2006) pose hover as an inverse problem and find optimum wing kinematics that achieve this.

By manipulating wing kinematics in a certain way, desired aerodynamic forces are produced, the insect is able to steer its body favorably. To be able to understand the interplay between aerodynamic forces and the body dynamics, many researchers have developed mathematical models of insect flight. Following methods have been universally adopted for the analysis. The equations governing the motion of the body are written in standard aircraft equations of motion form, i.e. nonlinear and 6 degrees of freedom for the body. Under certain assumptions, the longitudinal and lateral motion are decoupled, as is done in aircraft analysis. This reduces the analysis to two 3 DOF subsystems, and hence easier. One of the assumptions made, which is

almost universally adopted, is that the wing inertia effect on body is small enough to be ignored. The wings degrees of freedom are not modeled. This greatly simplifies the analysis of the system further. Few researchers e.g. Sun *et al.* (2007), Taha (2013) and Orlowski and Girard (2011b), modeled the wing and its effect on the body. In fact, Orlowski and Girard (2011b) and Bolender (2009) conclude that the wing inertial effect should be taken into consideration while modeling the dynamics of the system.

The wings provide the actuating force, and since wings flap in a periodic manner, the force on the body is periodic. Since the force vector field is non autonomous, the system of equations of motion becomes time varying. To deal with the time varying nature of the differential equations, two approaches are used: *Floquet theory* or Averaging. Using the former entails, finding a periodic orbit (solution) that satisfies the time varying differential equations and then linearizing the system about this orbit. Stability is determined by the eigenvalues (*Floquet multipliers*) of the system *'A'* matrix. This approach has been used by Dietl and Garcia (2008) Averaging theory, on the other hand, predicts the behavior of the original time varying system 'on an average'. Averaging technique is the more popular choice for analyzing the system as opted by Oppenheimer *et al.* (2011), Deng *et al.* (2006a), Khan and Agrawal (2007), Orlowski and Girard (2011a), Karásek and Preumont (2012). Averaging for flapping wing MAVs have been dealt with rigorously in Deng *et al.* (2006a).

An insect employs active control to follow a desired flight condition. Reiterating some of the important parameters that insects employ for flight control are: the stroke plane angle, flapping amplitude, offset and frequency and lastly wing pitching angle magnitude in both upstroke and downstroke and timing of stroke reversal. A good description of how an insect steers itself is given in Taylor (2001). To be able to mimic insect flight, some of the listed parameters have been chosen as control parameters for MAVs. The relative importance of these control parameters change from hover

state to forward flight as noted by several biologists (Wu and Sun (2009)). Thus flight condition is an important aspect to keep in mind that determines the usage of these controls. As a way of testing the flight control algorithms, physics engine module was used by Dickson *et al.* (2008). Sensors and actuators were modeled too in this paper. Similar work can be found in Deng *et al.* (2006a) and Epstein *et al.* (2007). Body dynamics with sensors like *Haltere* dynamics were incorporated and simpulation results have been shown.

1.2 Outline of the Thesis

In this thesis, we base our MAV model on a Hawk moth, which turns out to be an interesting model. The two main assumptions, i.e. neglecting wing mass and averaging the time varying equations of motion, are in question because the Hawk moth has heavier wings compared to other insects (6% of body weight) and it also flaps at a much lower frequency (30 Hz) than other insects (Willmott and Ellington (1997a). Secondly, Averaging is valid when the one system's dynamics is sluggish, compared to the second system driving it. Here the two systems are the body (slow) and the wing. In other words, the bandwidth of the body is sufficiently small compared to the bandwidth of the wing. However the assumption that the body's dynamics will be dictated by the averaged wing force comes into question when the difference between the two bandwidths is small. Taha (2013) show that when the model has a very small wing beat frequency making it close to the natural frequency of the body (ratio of the two is less than 100), higher order averaging might be necessary to get a better approximation. The main contribution of this thesis is to address partially answered questions about the two main concerns mentioned above.

1. When is the mass-less wing model sufficient? When does it become necessary to include it in the model?

2. In a feedback system, how robust can the controller be made to these modeling uncertainties? How much wing mass can be tolerated beyond which the controller fails to stabilize the system?

3. When does first order averaging work?

4. When is it absolutely necessary to bring in higher order averaging terms?

These questions were posed by Sun *et al.* (2007) and answered using CFD analysis. Few researches have claimed that wing inertia effect on the body should not be ignored and it can change the dynamics by a big margin (Bolender (2009)). With regards, to averaging, Taha (2013) claims the difference between the frequencies should be at least 100. Conservatism on these claims/bound needs to be questioned. Most of the work mentioned here were done on a system without feedback control i.e. open loop. In this work, we have tried giving rules of thumb from a controls perspective.

We now give a brief overview of the forthcoming chapters; The basic mechanism of insect flight is reviewed in chapter 2, an aerodynamic model is developed and the complete rigid body, nonlinear equations of motion is presented. In this chapter three models i.e. model without wing inertial effect on body, model with wing inertial effect on body and the complete system consisting of body and wings, have been derived using Newton's equations. In chapter 3, a short introduction to averaging theory has been given. Both first and higher order averaging for periodic case are covered; and what it results for the MAV system. In chapter 4, linearized approximation of the model around hover is derived and linear analysis is done for the models. In chapter 5, LQR controller has been designed. Closed loop maps and controller trade-offs are examined. The controller for first model, i.e. model without wing inertial effect, is tested for its robustness, by making it work on model 2, i.e with the wing inertial effect. chapter 6, concludes the thesis and reviews possibilities for future research.

Chapter 2

THE NON-LINEAR TIME PERIODIC MODEL

2.1 Flapping Flight in Insects

In this short introduction, we look at the mechanism of insect flight that will aid us in modeling. Be it an aircraft or a bird, the underlying principle of any flight is the same, i.e. the aerodynamic lift counters the weight while thrust counters drag and provides propulsion. But the way a bird's flight is different from an aircraft, is in the nature of their lift production. In a typical aircraft, the wing's pitch provides the angle of attack and the lift generated is proportional to the magnitude of this angle of attack, while the engines provide thrust. Similarly in flying insects and birds, the wing pitches to provide angle of attack and it flaps periodically to provide thrust. Insects are very different from birds, in their flying mechanisms. Insects are able to produce lift 2-3 times in excess of their body weight. A bird flaps its wings up and down. During the downstroke, the wing pushes the air downwards, generating lift. When an insect wing flaps, its front edge goes down and forward and then does almost 90° flip, and continues up and backward, tracing a flattened figure eight. This motion leads the insect wing to attack the oncoming air at a high angle. This is where the biggest difference between an airplane wing comes, an airplane wing has a relatively small angle of attack, almost parallel to the direction of travel. Increasing the angle, increases the lift, but only up to a point. Beyond this point of maximum lift, tilting the leading edge any further, results in a separation of the airflow from the upper surface and the lift vanishes. This phenomenon is called *stalling*. However, the insect wing, is always on the edge of stalling, the point of maximum lift. This

stalling leads to the formation of a large vortex on the wing, called the *leading edge vortex* (Ellington *et al.* (1996)). This generates 70% of the lift. At the end of each downstroke and upstroke, as the wing is about to make the rotation, of the figure eight, it sheds the leading-edge vortex. The rotation accelerates the airflow over the top of the wing, thus generating a burst of even greater lift. By controlling the timing of those wing flips, the insect can steer the direction of the lift (Dickinson *et al.* (1999)).

Alexander (2004) and Dudley (2002) are good references for understanding physiology and mechanism of animal flight in detail. Kinematics of the wing play a major role in shaping the aerodynamic force to produce a desirable outcome (Sane and Dickinson (2001). Insects typically flap in a plane called stroke plane which is oriented at a *stroke plane angle* β from the longitudinal axis of the body. The lift and drag produced by the wing are perpendicular and parallel to this plane. Insects increase β to accelerate forward and make it negative to decelerate or fly backwards. Similarly accelerations in lateral direction result from rolling of the stroke plane. Tilting of the stroke plane, results in rotation of the lift vector (as will be explained next), and thus small tilts produce substantial horizontal thrusts (Ellington (1984b)). As the forward velocity increases, the stroke plane becomes more and more vertical, and the body angle reduces, becoming more and more horizontal. This is to reduce body drag. The angle between the stroke plane and the body almost remains constant.

The aerodynamic force produced by the wing is proportional to the angle of attack and square of the velocity with which it is moving. As a result, the force produced in the downstroke is more than that of the upstroke, this is because the relative velocity of the wing on the downstroke is higher (assuming the body is moving in the direction of downstroke i.e. forward in the figure 2.1). However the propelling force (thrust component) comes from the upstroke. To compensate for low velocity in the upstroke,

the angle of attack in the upstroke increases. As a direct consequence of this, as the forward velocity increases, downstroke becomes more and more horizontal, while the upstroke becomes more vertical, so that the thrust vector (in upstroke) is oriented in the direction of movement. This difference in magnitude of the force is possible because the wing assumes different pitch angles α_d and α_u in each half stroke. Stroke plane angle plays a major role in this asymmetry. At small β angle, the asymmetry is larger.

For the sake of clarity, the above discussion has been repeated here but with force resolution shown in figure 2.1. Lift, drag and the resultant produced in the down stroke are denoted as $\mathbf{L_d}$, $\mathbf{D_d}$ and $\mathbf{R_d}$ respectively, similar nomenclature is used in the upstroke. The total resultant of, each stroke's resultant $\mathbf{R_d}$ and $\mathbf{R_u}$ is denoted as $\mathbf{R}$. The components of $\mathbf{R}$ along body's x_b and z_b direction decides the direction of body's movement. In hover, $\mathbf{R_z}$ should counter the weight and $\mathbf{R_x}$ should be zero. If the two strokes are symmetrical, the forces in the plane (i.e. horizontal), cancel each other out. For forward flight to be possible, $\mathbf{R_x}$ plays the role of thrust and should be in the direction of desired movement. β decides the tilt of the resultant force vector, hence the more tilt the more thrust. It is now clear from figure 2.1 that most of the thrust is generated in upstroke and since the magnitude is directly proportional to the angle of attack, the angle of attack is higher in the up stroke than in the down stroke. This differential angle of attack is very essential in forward flight.

2.2 Dynamic Model

In this section the complete equations of motion for the MAV system have been derived. By complete we mean body and two rigid wings. For sake of simplicity, equations of motion for the system without wings has been derived first, which are the standard aircraft equations. Next the system with wings has been dealt with.

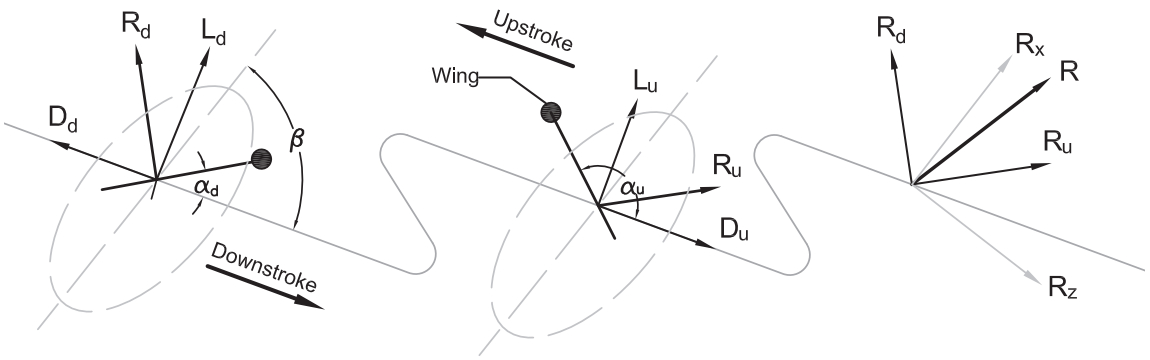

Figure 2.1: Force Resolution in Upstroke and Downstroke

Various representations have been used to model the equations of motion. In this thesis, the equations have been written in standard Newton's method.

2.2.1 Geometry

The MAV is modeled after a Hawkmoth insect. The body and wing parameters are given in the table. The parameters have been given in Ellington (1984a). The body is modeled as a cylinder of length L and constant radius of r_1. The wings hinge point is assumed to be aligned with the body's longitudinal axis. This dimension is marked as l_1 which is varied from the given length to zero to check its effect in later chapters. In the configuration, when the wing hinge is aligned with the C.G, symmetric flapping would result in zero average moment about the body's C.G, and pitch control would be lost. Thus, to regain pitch control, unsymmetrical flapping of wings would have to be adopted. In this thesis as seen later, an offset term in the flapping function will be introduced, to achieve this. If the flapping offset is such that the wing lies mostly in front of the body, then pitch up moment is created and if the wing flaps mostly behind the body, the pitch down moment is created. The body's center of pressure lies behind the C.G along the longitudinal axis, this dimension is marked as l_2. The wings are modeled as rectangular plates with length and width b_w

and c_w.

Table 2.1: Physical Parameters

Mass (M_b)	1554 mg
Moment of inertia about y_b axis (I_{by})	2.435 $\times 10^{-7}$ kg m^2
Wing mass (M_w)	47 mg
Wing semispan (b_w)	51.9 mm
Wing chord (c_w)	18.4 mm
Normalized centre of pressure ($\hat{r}_2$)	0.525
Body length (L)	42.1 mm
Radius of Body (r_1)	6 mm
Wing hinge 'x' coordinate from the C.G (l_1)	$0.2846L$
Radius of gyration (l_2)	$0.3676L$
Area of wing (A_w)	947.8 mm^2

2.2.2 Equations of Motion for Body Without Wings

The derivation presented in this section is similar to the models presented in works like Khan and Agrawal (2005), Faruque and Sean Humbert (2010), Oppenheimer *et al.* (2011) and so on. The central body typically has 6 degrees of freedom, 3 translational and 3 rotational and the wings, each have 3 additional rotational degrees of freedom, but are constrained to move with the body. Since in this work only hovering and forward flight regimes have been studied, both of which are longitudinal flight condition, we restrict the dynamic model to this plane (3 DOF). This restricts both left and right wing to have the same motion, any unsymmetrical motion would lead to out of plane reaction. Five frames are typically used to capture the motion,

inertial frame (x_e, y_e, z_e), body frame (x_b, y_b, z_b), stroke plane frame (x_{sp}, y_{sp}, z_{sp}), this is the frame in which the stroke takes place, an intermediate flapping plane to capture the position of the wing in the stroke plane (x'_{sp}, y'_{sp}, z'_{sp}) and lastly wing frame (x_w, y_w,z_w). Both the stroke plane and wing frame have their origins at the wing hinge. Since we are primarily interested in the body's motion, the equations of motion are written in the body frame.

Angle θ, measured from the positive x_e, gives the absolute position of the body w.r.t to the inertial frame. The stroke plane frame is oriented at an angle β measured with respect to positive x_b. β can take values from $[-\pi/2\ \pi/2]$. The stroke plane angle β is held constant for a particular flight condition. The wing has 3 rotational degrees of freedom, thus the wing position w.r.t to the stroke plane is given by 3 angles, but in this work only 2 degrees of freedom have been considered i.e. flapping and pitching. Flapping ϕ, is the rotation made about the z_{sp} axis, pitching α, the rotation about the y'_{sp} axis. The coordinate frames are shown in 2.2. *Note the β shown in the figure is negative.*

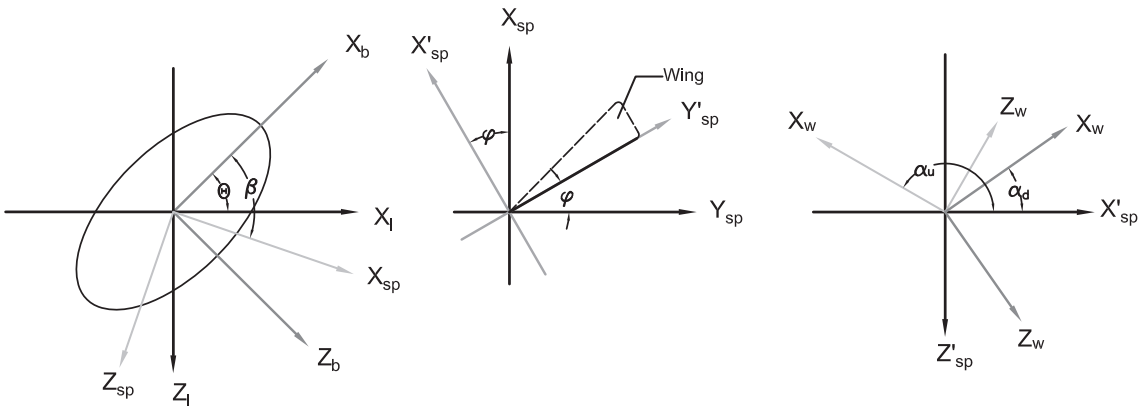

Figure 2.2: Coordinate Frames

The rotation matrix from inertial frame to the body frame is

$$R_\theta = \begin{bmatrix} \cos\theta & 0 & -\sin\theta \\ 0 & 1 & 0 \\ \sin\theta & 0 & \cos\theta \end{bmatrix} \tag{2.1}$$

The rotation matrices from body frame to stroke frame, stroke frame to intermediate frame, and finally from intermediate frame to wing frame are as follows

$$R_\beta = \begin{bmatrix} \cos\beta & 0 & -\sin\beta \\ 0 & 1 & 0 \\ \sin\beta & 0 & \cos\beta \end{bmatrix} \; R_\phi = \begin{bmatrix} \cos\phi & \sin\phi & 0 \\ -\sin\phi & \cos\phi & 0 \\ 0 & 0 & 1 \end{bmatrix} \; R_\alpha = \begin{bmatrix} \cos\alpha & 0 & -\sin\alpha \\ 0 & 1 & 0 \\ \sin\alpha & 0 & \cos\alpha \end{bmatrix} \tag{2.2}$$

The rotation matrix from the body to the wing frame and vice versa are given by

$$\begin{aligned} \underset{bw}{R} &= R_\alpha R_\phi R_\beta \\ \underset{wb}{R} &= \underset{bw}{R}^T \end{aligned} \tag{2.3}$$

Having defined the geometry and the coordinate frames, we now write the equations of motion. Let us define the following quantities in the body frame:

$\mathbf{F}$, $\mathbf{M}$	Total force and total moment acting at the body's C.G
$\mathbf{F}_a$ and $\mathbf{M}_a$	Aerodynamic forces and moments of the wing
$\mathbf{F}_b$ and $\mathbf{M}_b$	Aerodynamic forces and moments of the body
$\mathbf{V}_b$ and ω_b	Velocity and angular velocity of the body

The equations of motion, written in the body frame (subscript denotes the frame) are

$$\begin{aligned} \mathbf{F} &= M_b\Big(\underset{b}{\frac{\partial \mathbf{V}_b}{\partial t}} + \omega_b \times \mathbf{V}_b\Big) \\ \mathbf{M} &= I_b\Big(\underset{b}{\frac{\partial \omega_b}{\partial t}}\Big) + \omega_b \times I_b\omega_b \end{aligned} \tag{2.4}$$

where I_b is the body inertia tensor.

In the equations derived in this section, only forces from the wings have been considered because at hover, the aerodynamic forces acting on the body (parasitic drag and lift) are negligible, but for forward flight, these have to be included too as shown below:

F and **M** are defined as below

$$\mathbf{F} = \mathbf{F_a} - \mathbf{F_b} + R_\theta \begin{bmatrix} 0 \\ 0 \\ g \end{bmatrix} = \begin{bmatrix} F_x \\ F_y \\ F_z \end{bmatrix} + g \begin{bmatrix} -\sin\theta \\ 0 \\ \cos\theta \end{bmatrix}$$

$$\mathbf{M} = \mathbf{M_a} - \mathbf{M_b} = \begin{bmatrix} M_x \\ M_y \\ M_z \end{bmatrix} \tag{2.5}$$

Thus the complete equations of motion for the body alone, in the longitudinal plane are

$$\begin{aligned} \dot{u} &= \frac{F_x}{M_b} - g\sin\theta - qw \\ \dot{w} &= \frac{F_z}{M_b} + g\cos\theta + qu \\ \dot{\theta} &= q \\ \dot{q} &= \frac{M_y}{I_{by}} \end{aligned} \tag{2.6}$$

2.2.3 Equations of Motion for Body with Wings

In this section we derive the equations of motion for the complete system i.e. body plus wings. *An important point to remember is that the following equations of motion have been derived considering one wing, as long as we restrict the motion to longitudinal plane, the kinematics of the other wing would remain the same, thus enabling us to write the equations for one wing and extending it to the other by simply*

multiplying the respective terms by 2.

We start by defining the inertia tensor of one wing. The inertia tensor for other wing would be identical. It is calculated at the wing hinge according to

$$I_w = \begin{bmatrix} \frac{M_w}{3} b_w^2 & 0 & 0 \\ 0 & \frac{M_w}{12} c_w^2 & 0 \\ 0 & 0 & M_w(\frac{b_w^2}{3} + \frac{c_w^2}{12}) \end{bmatrix} \tag{2.7}$$

To start the derivation following vectors need to be defined

$\mathbf{R_h}$	Vector from the body C.G to the wing hinge, in body frame
$\mathbf{R_w}$	Vector from the wing hinge to the wing C.G, in wing frame
$\mathbf{V_b}$, $\mathbf{V_h}$	Absolute velocities of the body center of mass and wing hinge (w.r.t inertial frame), in body frame
$\mathbf{V_w}$	Relative velocity of wing center of mass w.r.t hinge, in body frame
ω_b	Angular velocity of the body, in body frame
ω_w	Angular velocity of the wing, in wing frame
${}_b\omega_w$	Angular velocity of the wing in body frame
ω_{w0}	Angular velocity of the wing relative to the body in wing frame
$\mathbf{H}_b$, $\mathbf{H}_w$	Angular momentum of body in body frame and wing in wing frame respectively

where,

$$\omega_w = \underset{bw}{R}\omega_b + \omega_{w0} \tag{2.8}$$

We write the equations of motion for the body by summing up the total force and moment acting at the C.G (Greenwood (1988)). Note the subscripts denote the frame in which the vector lies.

$$\mathbf{F} = M_b(\frac{d\mathbf{V_b}}{dt}) + M_w\Big(\frac{d\mathbf{V_h}}{dt} + \frac{d\mathbf{V_w}}{dt}\Big) \tag{2.9}$$

$$\mathbf{M} = M_w\Big((\mathbf{R_h} + \mathbf{R_w}) \times \frac{d\mathbf{V_h}}{dt} + \mathbf{R_h} \times \frac{d\mathbf{V_w}}{dt}\Big) + \frac{d\mathbf{H}_b}{dt} + \frac{d\mathbf{H}_w}{dt} \tag{2.10}$$

Expressions for velocities and accelerations are as follows:

$$\mathbf{V_h} = \mathbf{V_b} + {}_b\frac{\partial \mathbf{R_h}}{\partial t} + \omega_b \times \mathbf{R_h} = \mathbf{V_b} + \omega_b \times \mathbf{R_h} \tag{2.11}$$

$${}_w\mathbf{V_w} = {}_w\frac{\partial \mathbf{R_w}}{\partial t} + (\omega_w \times \mathbf{R_w}) = \omega_w \times \mathbf{R_w} \tag{2.12}$$

$$\frac{d\mathbf{V_h}}{dt} = {}_b\frac{\partial \mathbf{V_b}}{\partial t} + \omega_b \times \mathbf{V_b} + {}_b\frac{\partial \omega_b}{\partial t} \times \mathbf{R_h} + \omega_b \times (\omega_b) \times \mathbf{R_h} \tag{2.13}$$

$${}_w\frac{d\mathbf{V_w}}{dt} = {}_w\frac{\partial \omega_w}{\partial t} \times \mathbf{R_w} + \omega_w \times (\omega_w \times \mathbf{R_w}) \tag{2.14}$$

In the above equations, vectors from two different frames, body and wing frame, were used (see equation 2.12, 2.14). To bring all the terms in the same frame i.e. body frame, rotation matrices are used as shown

$${}_b(\omega_w \times \mathbf{R_w}) = \underset{wb}{R}{}_w(\omega_w \times \mathbf{R_w}) \tag{2.15}$$

$${}_b\big({}_w\frac{\partial \omega_w}{\partial t} \times \mathbf{R_w} + \omega_w \times (\omega_w \times \mathbf{R_w})\big) = \underset{wb}{R}{}_w\big({}_w\frac{\partial \omega_w}{\partial t} \times \mathbf{R_w} + \omega_w \times (\omega_w \times \mathbf{R_w})\big) \tag{2.16}$$

Substituting (2.11-2.16) in (2.9) and (2.10),

$$\begin{aligned}\mathbf{F} = M_t({}_b\frac{\partial \mathbf{V_b}}{\partial t}) + M_t(\omega_b \times \mathbf{V_b}) + M_w\Big({}_b\frac{\partial \omega_b}{\partial t} \times \mathbf{R_h} + \omega_b \times (\omega_b \times \mathbf{R_h}) \\ + \underset{wb}{R}({}_w\frac{\partial \omega_w}{\partial t} \times \mathbf{R_w} + \omega_w \times (\omega_w \times \mathbf{R_w})\Big)\end{aligned} \tag{2.17}$$

where, M_t is the total mass, body plus wing

$$\begin{aligned}\mathbf{M} = M_w\Big(\big(\mathbf{R_h} + \underset{wb}{R}\mathbf{R_w}\big) \times \big({}_b\frac{\partial \mathbf{V_b}}{\partial t} + \omega_b \times \mathbf{V}_b + {}_b\frac{\partial \omega_b}{\partial t} \times \mathbf{R_h} + \omega_b \times (\omega_b \times \mathbf{R_h})\big)\Big) \\ + M_w\Big(\mathbf{R_h} \times \underset{wb}{R}\big({}_w\frac{\partial \omega_w}{\partial t} \times \mathbf{R_w} + \omega_w \times (\omega_w \times \mathbf{R_w})\big)\Big) + {}_b\frac{d\mathbf{H}_b}{dt} + {}_b\frac{d\mathbf{H}_w}{dt}\end{aligned} \tag{2.18}$$

where,

$${}_b\frac{d\mathbf{H}_b}{dt} = I_b\big({}_b\frac{\partial \omega_b}{\partial t}\big) + \omega_b \times I_b\omega_b \tag{2.19}$$

$${}_w\frac{d\mathbf{H}_w}{dt} = I_w\big({}_w\frac{\partial \omega_w}{\partial t}\big) + \omega_w \times I_w\omega_w \tag{2.20}$$

$${}_b\frac{d\mathbf{H}_w}{dt} = \underset{wb}{R}\big(I_w({}_w\frac{\partial \omega_w}{\partial t}) + \omega_w \times I_w\omega_w\big) \tag{2.21}$$

Up until here the equations derived are for the body alone, with wing inertial effect modeled in it. Similar derivation of these equations is given in Sun *et al.* (2007).

The wing's motion is described with respect to the stroke plane frame, thus for convenience, the wing equations of motion are written in this frame. We start by defining the following vectors in the stroke plane

- τ Total torque acting on the wing at the hinge
- τ_g Torque due to gravity
- τ_α Component of input torque in y'_{sp} direction
- τ_ϕ Component of input torque in z_{sp} direction

The total moment acting at the wing hinge is given as

$$\tau + \tau_g = M_w\Big(({}_{w-sp}R\,\mathbf{R_w}) \times R_\beta({}_b\frac{d\mathbf{V}_h}{dt})\Big) + R_\beta({}_b\frac{d\mathbf{H}_w}{dt}) \tag{2.22}$$

$$\tau + \tau_g = M_w\Big(({}_{wsp}R\,\mathbf{R_w}) \times R_\beta({}_b\frac{\partial \mathbf{V_b}}{\partial t} + \omega_b \times \mathbf{V}_b + {}_b\frac{\partial \omega_b}{\partial t} \times \mathbf{R_h} + \omega_b \times (\omega_b \times \mathbf{R_h}))\Big) + R_\beta({}_b\frac{d\mathbf{H}_w}{dt}) \tag{2.23}$$

The equations derived till here, are for the general case i.e. 6 DOF (3 translational and 3 rotational) for the body and 3 DOF (rotational) for the wing. Restricting to the longitudinal plane (3 DOF), simplifies the equations. Control of longitudinal and lateral movement is possible by allowing 2 DOF for the wings i.e. flapping and pitching. The third DOF (deviation angle) has not been considered here. The significance of the third DOF in insects too, is small (Ellington (1984b)). Most of the work published in MAV research, is in accordance with this. Since motion is restricted to the longitudinal frame, the wing motion is symmetrical about the longitudinal axis, thus the left wing undergoes the same motion as the right one. The equations given

below are written for the right wing, the equations for the left wing would remain the same. We simplify the equations 2.17, 2.18 and 2.23 for longitudinal and 2 DOF wing case below. These equations have been used in this thesis for further work.

We start by defining the flapping degree of freedom, i.e. the rotation about z_{sp}. The wing flaps back and forth, in a periodic manner. The flap closely resembles a sinusoid, thus the *sin* function has been the most popular choice.

$$\phi(t) = \phi_o - \phi_m \sin(\omega t) \tag{2.24}$$

where ϕ_m is the mean flapping angle and ϕ_o is the offset. The sin is negative here because it is written for the right wing which makes a negative angle when it flaps forward (down stroke). However the left wing makes a positive angle during down-stroke, it is so because of the way the axes are set up. The pitch angle assumes two different magnitudes in upstroke and downstroke. Here, it is described by hyperbolic tan function but a cosine or a signum function also serve the purpose.

$$\alpha(t) = (\alpha_m - \frac{\pi}{2}) \tanh(4.5 \sin(\omega t + \frac{\pi}{2})) + (\alpha_o + \frac{\pi}{2}) \tag{2.25}$$

Enumerating the vectors used in the equations of motion (some are repeated from the previous wingless model for convenience).

u, w	components of body's velocity in x_b and z_b directions
q	component of body's angular velocity in y_b direction
θ	rotation angle of the body about y_b direction
ϕ	rotation angle of the wing about z_{sp} direction
α	rotation angle of the wing about z'_{sp} direction
β	rotation angle of the stroke plane about y_b direction

Having defined the angles, we define the angular velocity of the wing relative to

the body in the wing frame as:

$$ {}_{w}\frac{\partial \omega_{w0}}{\partial t} = \begin{bmatrix} \ddot{\phi}\sin\alpha \\ \ddot{\alpha} \\ \ddot{\phi}\cos\alpha \end{bmatrix} \tag{2.26} $$

The stroke plane angle β is considered to be fixed for a particular flight condition. Thus, derivatives of β are set to zero, and there is no angular velocity of stroke plane rotation.

The geometrical parameters are defined as:

$$ \mathbf{R_w} = \begin{bmatrix} 0 & \frac{b_w}{2} & 0 \end{bmatrix}^T, \ \mathbf{R_h} = \begin{bmatrix} l_1 & r_1 & 0 \end{bmatrix}^T \tag{2.27} $$

The above dimensions are have been written for the right wing, the left wing will have the same magnitude but with negative y coordinate.

Substituting equations 2.26 and 2.27 in equations (2.17), (2.18) and (2.23) we get the final equations in the following form:

$$ [M](\dot{\mathbf{x}}) = [\mathbf{F}] \tag{2.28} $$

where, $\mathbf{x} = \begin{bmatrix} u & w & \theta & q & \alpha & \dot{\alpha} & \phi & \dot{\phi} \end{bmatrix}^T$

$$ M = \begin{bmatrix} M_t & 0 & 0 & m14 & 0 & 0 & 0 & m18 \\ 0 & M_t & 0 & m24 & 0 & 0 & 0 & m28 \\ 0 & 0 & 1 & 0 & 0 & 0 & 0 & 0 \\ m14 & m24 & 0 & m44 & 0 & m46 & 0 & m48 \\ 0 & 0 & 0 & 0 & 1 & 0 & 0 & 0 \\ -m14 & m62 & 0 & m64 & 0 & m46 & 0 & m68 \\ 0 & 0 & 0 & 0 & 0 & 0 & 1 & 0 \\ m18 & m28 & 0 & m48 & 0 & 0 & 0 & m88 \end{bmatrix} $$

$$m14 = M_w r \sin\beta \sin\phi$$

$$m18 = -M_w r \cos\beta \cos\phi$$

$$m24 = M_w r \cos\beta \sin\phi - M_w l_1$$

$$m28 = M_w r \sin\beta \cos\phi$$

$$m44 = -2M_w r l_1 \cos\beta \sin\phi + M_w l_1^2 + I_{by} + (I_{wx} \cos^2\alpha + I_{wz} \sin^2\alpha) \sin^2\phi + I_{wy} \cos^2\phi$$

$$m46 = -I_{wy} \cos\phi$$

$$m48 = -M_w r l_1 \sin\beta \cos\phi + (-I_{wx} + I_{wz}) \sin\phi \sin\alpha \cos\alpha$$

$$m62 = -M_w r \cos\beta \sin\phi$$

$$m64 = M_w r l_1 \cos\beta \sin\phi + I_{wx} \sin^2\phi \cos^2\alpha + I_{wy} \cos^2\phi + I_{wz} \sin^2\phi \sin^2\alpha$$

$$m66 = (-I_{wx} + I_{wz}) \sin\phi \sin\alpha \cos\alpha$$

$$m88 = I_{wx} \sin^2\alpha + I_{wz} \cos^2\alpha$$

$$
F = \begin{bmatrix}
F_x - M_t g \sin\theta - M_t q w \\
-M_w(q^2 \frac{b_w}{2} \cos\beta \sin\phi - q^2 l_1 + 2q\dot{\phi}\frac{b_w}{2} \sin\beta \cos\phi + \dot{\phi}^2 \frac{b_w}{2} \cos\beta \sin\phi) \\
F_z + M_t g \cos\theta + M_t q u \\
-M_w(-q^2 \frac{b_w}{2} \sin\beta \sin\phi + 2q\dot{\phi}\frac{b_w}{2} \cos\beta \cos\phi - \dot{\phi}^2 \frac{b_w}{2} \sin\beta \sin\phi) \\
q \\
M_y - M_w\big(qw\frac{b_w}{2} \sin\beta \sin\phi - qu(l_1 - \frac{b_w}{2} \cos\beta \sin\phi) \\
+\dot{\phi}^2 \frac{b_w}{2} l_1 \sin\beta \sin\phi - 2q\dot{\phi}\frac{b_w}{2} l_1 \cos\beta \cos\phi + g \sin\theta \frac{b_w}{2} \sin\beta \sin\phi \\
-g \cos\theta(l_1 - \frac{b_w}{2} \cos\beta \sin\phi)\big) - I_{wx}(-2q\dot{\alpha} \sin^2\phi \sin\alpha \cos\alpha \\
+2q\dot{\phi} \sin\phi \cos\phi \cos^2\alpha - \dot{\phi}^2 \cos\phi \sin\alpha \cos\alpha + \dot{\phi}\dot{\alpha} \sin\phi \sin^2\alpha \\
-\dot{\phi}\dot{\alpha} \sin\phi \cos^2\alpha) - I_{wy}(-2q\dot{\phi} \sin\phi \cos\phi - \dot{\phi}\dot{\alpha} \sin\phi) \\
-I_{wz}(2q\dot{\alpha} \sin^2\phi \sin\alpha \cos\alpha + 2q\dot{\phi} \sin\phi \cos\phi \sin^2\alpha + \dot{\phi}^2 \cos\phi \sin\alpha \cos\alpha \\
+\dot{\phi}\dot{\alpha} \sin\phi \cos^2\alpha - \dot{\phi}\dot{\alpha} \sin\phi \sin^2\alpha) \\
\dot{\alpha} \\
\tau_\alpha \cos\phi + M_{wy} + M_w g \frac{b_w}{2} \sin\phi(-\sin\theta \sin\beta + \cos\theta \cos\beta) \\
-M_w(-qw\frac{b_w}{2} \sin\beta \sin\phi + q^2 \frac{b_w}{2} l_1 \sin\beta \sin\phi + qu\frac{b_w}{2} \cos\beta \sin\phi) \\
-I_{wx}(-2q\dot{\alpha} \sin^2\phi \sin\alpha \cos\alpha + 2q\dot{\phi} \sin\phi \cos\phi \cos^2\alpha - \dot{\phi}^2 \cos\phi \\
\sin\alpha \cos\alpha + \dot{\phi}\dot{\alpha} \sin\phi \sin^2\alpha - \dot{\phi}\dot{\alpha} \sin\phi \cos^2\alpha) - I_{wy}(-2q\dot{\phi} \sin\phi \cos\phi \\
-\dot{\phi}\dot{\alpha} \sin\phi) - I_{wz}(2q\dot{\alpha} \sin^2\phi \sin\alpha \cos\alpha + 2q\dot{\phi} \sin\phi \cos\phi \sin^2\alpha \\
+\dot{\phi}^2 \cos\phi \sin\alpha \cos\alpha + \dot{\phi}\dot{\alpha} \sin\phi \cos^2\alpha - \dot{\phi}\dot{\alpha} \sin\phi \sin^2\alpha) \\
\dot{\phi} \\
\tau_\phi + M_w g \frac{b_w}{2}(\sin\theta \cos\beta + \cos\theta \sin\beta) + M_{wz} \\
-M_w(-qw\frac{b_w}{2} \cos\beta \cos\phi + q^2 \frac{b_w}{2} l_1 \cos\beta \cos\phi - qu\frac{b_w}{2} \sin\beta \cos\phi) \\
-I_{wx}(q\dot{\alpha} \sin\phi \sin^2\alpha - q\dot{\alpha} \sin\phi \cos^2\alpha + 2\dot{\phi}\dot{\alpha} \sin\alpha \cos\alpha \\
-q^2 \sin\phi \cos\phi \cos^2\alpha) - I_{wy}(q\dot{\alpha} \sin\phi + q^2 \sin\phi \cos\phi) \\
-I_{wz}(-q\dot{\alpha} \sin\phi \sin^2\alpha + q\dot{\alpha} \sin\phi \cos^2\alpha - 2\dot{\phi}\dot{\alpha} \sin\alpha \cos\alpha \\
-q^2 \sin\phi \cos\phi \sin^2\alpha)
\end{bmatrix}
$$

This is the complete set of equations of motion for the entire system i.e. wing plus body. Two models have been derived here, first without wings i.e. equation (2.6) and second with wings (2.28).

2.2.4 Models for Control

In this section, the models used in the next 2 chapters will be revisited. Model 1 excludes the wing and its effect on the body, it encompasses just the body's equations of motion under the influence of periodic wing force (equation 2.6).

Model 2 again excludes the wing dynamics, and but includes the kinematics i.e. body's equations of motion with wing inertial effect (i.e. the first four equations of 2.28). Similar model was derived by Sun *et al.* (2007). But for simplification dynamics of wing pitch angle α have been ignored. However wing pitch angle serves as a control parameter. Model 2 has been repeated for sake of clarity in equation 3.12

Model 3 includes both body and wing dynamics, i.e. equation 2.28 but without α dynamics. In this model the wing kinematics are not imposed on the body, instead the wing dynamics, introduced as states, decide the kinematics.

$$\begin{bmatrix} M_t & 0 & 0 & m14 \\ 0 & M_t & 0 & m24 \\ 0 & 0 & 1 & 0 \\ m14 & m24 & 0 & m44 \end{bmatrix} \begin{bmatrix} \dot{u} \\ \dot{w} \\ \dot{\theta} \\ \dot{q} \end{bmatrix} =$$

$$F = \begin{bmatrix} F_x - M_t g \sin\theta - M_t q w \\ -M_w(q^2 \frac{b_w}{2} \cos\beta \sin\phi - q^2 l_1 + 2q\dot{\phi}\frac{b_w}{2} \sin\beta \cos\phi + \dot{\phi}^2 \frac{b_w}{2} \cos\beta \sin\phi) \\ F_z + M_t g \cos\theta + M_t q u \\ -M_w(-q^2 \frac{b_w}{2} \sin\beta \sin\phi + 2q\dot{\phi}\frac{b_w}{2} \cos\beta \cos\phi - \dot{\phi}^2 \frac{b_w}{2} \sin\beta \sin\phi) \\ q \\ M_y - M_w(qw\frac{b_w}{2} \sin\beta \sin\phi - qu(l_1 - \frac{b_w}{2} \cos\beta \sin\phi) \\ +\dot{\phi}^2 \frac{b_w}{2} l_1 \sin\beta \sin\phi - 2\dot{\phi}\frac{b_w}{2} l_1 \cos\beta \cos\phi \\ +g \sin\theta \frac{b_w}{2} \sin\beta \sin\phi - g \cos\theta \frac{b_w}{2} \cos\beta \sin\phi) \\ -I_{wx}(2q\dot{\phi} \sin\phi \cos\phi \cos^2\alpha - \dot{\phi}^2 \cos\phi \sin\alpha \cos\alpha \\ -I_{wy}(-2q\dot{\phi} \sin\phi \cos\phi - \dot{\phi}\dot{\alpha} \sin\phi) - I_{wz}(2q\dot{\phi} \sin\phi \cos\phi \sin^2\alpha \\ -\dot{\phi}^2 \cos\phi \sin\alpha \cos\alpha \end{bmatrix} \quad (2.29)$$

2.3 Aerodynamic Model

In this section, we develop the aerodynamic model. The model is based on Deng *et al.* (2006b). The body experiences two different sets of aerodynamic forces, first originating from the movement of the wings and the other due to its own motion in the air. The aerodynamic force due to the flapping of the wings, provides the actuation for the body, while the aerodynamic force due its own movement, known as parasitic force, do not provide any useful force, hence the name parasitic. If the wing actuation is sufficient enough, these parasitic forces are overcome and the body is propelled forward. Since the magnitude of the aerodynamic force is proportional

to the square of velocity, which is practically negligible at or near hover, the body forces do not account for a substantial amount and are ignored in this model.
Another point to note here is, that the angle of attack is strictly the angle made by the airfoil with the oncoming wind velocity vector. At hover or near hover, for all practical purposes, this is taken to be the pitch angle, but strictly speaking it is given by

$$\alpha_A = \alpha - \hat{\alpha} \ \ (\alpha = \alpha_d/\alpha_u) \tag{2.30}$$

$$\hat{\alpha} = \arctan(\frac{V_z}{V_x}) \tag{2.31}$$

The aerodynamic force lift and drag act along the relative velocity vector (as shown in figure 2.3 below), which makes an angle $\hat{\alpha}$. with the stroke plane angle. The rotation matrix from relative wind frame to stroke plane angle is given by

$$R_{\hat{\alpha}} = \begin{bmatrix} \cos\hat{\alpha} & 0 & -\sin\hat{\alpha} \\ 0 & 1 & 0 \\ \sin\hat{\alpha} & 0 & \cos\hat{\alpha} \end{bmatrix} \tag{2.32}$$

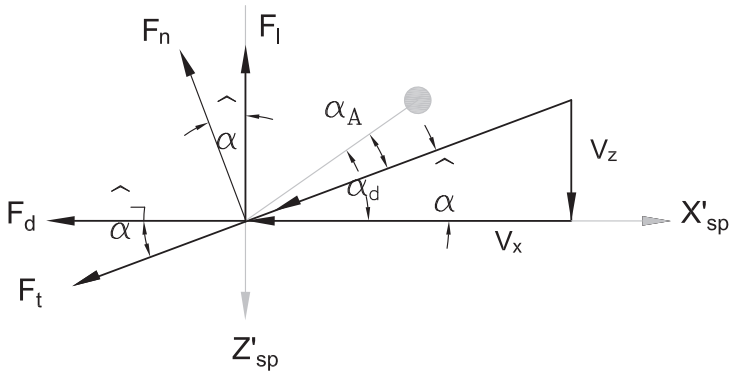

Figure 2.3: Angle of Attack Modification

The aerodynamic force, acts at the center of pressure. The vector from the wing

hinge to the center of pressure, in the body frame is given by:

$$\mathbf{R_{ac}} = R_\beta^T R_\phi^T R_\alpha^T \begin{bmatrix} \frac{c_w}{4} \\ \hat{r}_2 b_w \\ 0 \end{bmatrix} \tag{2.33}$$

The velocity of the center of pressure is the summation of total velocity of body and the rotational velocity of the wing in the intermediate wing frame is

$$\mathbf{U} = \underset{bw}{R}(\mathbf{V}_b + \omega_b \times \mathbf{R_h}) + (\underset{bw}{R}\omega_b + \omega_w \times \mathbf{R_{ac}}) \tag{2.34}$$

$$U_{cp}^2 = U_x^2 + U_z^2 \tag{2.35}$$

The quasi steady state approach has been widely used for modeling the aerodynamics forces. The model is derived from steady state, thin airfoil using blade element theory. The coefficients chosen here have been taken from Deng *et al.* (2006b). Force generated by the wing is due to 3 main phenomena, translation, rotation and delayed stall Dickinson *et al.* (1999). Here only the translational component has been modeled. The total force on the wing can be written as a function of angle of attack (α_A).

$$\begin{aligned} L &= \frac{1}{2}\rho A_w C_l U_c p^2 \\ D &= \frac{1}{2}\rho A_w C_d U_c p^2 \end{aligned} \tag{2.36}$$

where ρ is the density of air, A_w is the area of the wing and the lift and the drag coefficients are expressed in terms of the tangential and normal components as:

$$C_n = 3.4 \sin \alpha_A;$$

$$C_t = 0.4 \cos^2(2\alpha_A) \tag{2.37}$$

$$C_l = C_n \cos \alpha_A - C_t \sin \alpha_A$$

$$C_d = C_n \sin \alpha_A + C_t \cos \alpha_A \tag{2.38}$$

This is the total lift and drag generated by the wing in the relative wind frame.

The total force and moment acting at the C.G of the body is expressed in the body frame as

$$\mathbf{F} = R_\beta^T R_\phi^T R_{\hat{\alpha}}^T \begin{bmatrix} -D \\ 0 \\ -L \operatorname{sgn} \dot{\phi} \end{bmatrix} \tag{2.39}$$

$$\mathbf{M} = (\mathbf{R_h} + \mathbf{R_{ac}}) \times \mathbf{F} \tag{2.40}$$

The individual components of the forces are

$$F_x = \cos\beta \cos\phi(-D\cos\hat{\alpha} - L\sin\hat{\alpha}\operatorname{sgn}\dot{\phi}) + \sin\beta(D\sin\hat{\alpha} - L\cos\hat{\alpha}\operatorname{sgn}\dot{\phi}) \tag{2.41}$$

$$F_z = -\sin\beta\cos\phi(-D\cos\hat{\alpha} - L\sin\hat{\alpha}\operatorname{sgn}\dot{\phi}) + \cos\beta(D\sin\hat{\alpha} - L\cos\hat{\alpha}\operatorname{sgn}\dot{\phi}) \tag{2.42}$$

$$M_y = F_z R_{ac,x} - F_x R_{ac,z} \tag{2.43}$$

The aerodynamic forces and moments experienced by the wing in the stroke plane are

$${}_{sp}\mathbf{F} = R_\phi^T R_{\hat{\alpha}}^T \begin{bmatrix} -D \\ 0 \\ -L \operatorname{sgn} \dot{\phi} \end{bmatrix} \tag{2.44}$$

$$\tau =_{sp} \mathbf{R_{ac}} \times_{sp} \mathbf{F} \tag{2.45}$$

$$M_{wy} =_{sp} F_x \; {}_{sp}R_{ac,z} - \; {}_{sp}F_z \; {}_{sp}R_{ac,x} \tag{2.46}$$

$$M_{wz} =_{sp} F_y \; {}_{sp}R_{ac,x} - \; {}_{sp}F_x \; {}_{sp}R_{ac,y} \tag{2.47}$$

2.3.1 Body Forces

Body aerodynamic forces are modeled the same way as wing (equation 2.36). This force acts at the body center of pressure, which is at a distance l_2 from the body C.G.

$$L_b = \frac{1}{2}\rho A C_{lb} V^2$$
$$D_b = \frac{1}{2}\rho A C_{db} V^2 \tag{2.48}$$

where, A is the projected area of the body, C_{lb}, C_{db} are the aerodynamic coefficients and V is the magnitude of the total velocity experienced ($V^2 = u^2 + w^2$). The aerodynamic coefficients found in the literature are mostly for the wings. Willmott and Ellington (1997b) compare both wing and body coefficients (experimentally derived) over a range of velocities starting from hover for a hawkmoth.

Also the aerodynamic model presented in this section is strictly valid for hover. The coeffients usually decreases with increasing speed. Forward fight aerodynamics in insects like bumblebees and hawkmoths were studied by Dudley and Ellington (1990b) and Willmott and Ellington (1997b) respectively. The experiment of scaling *drosophila* wings and aping the wing trajectory to study hover was repeated by giving finite speed, to study effect of forward flight in Dickson and Dickinson (2004). This concludes the discussion on aerodynamic modeling of flapping wing MAVs.

2.4 Summary

We have derived 3 different models with increasing complexity. The first model i.e. without wing has been the most popular choice, for obvious reasons, it tremendously simplifies the modeling. However, strictly speaking, ignoring the wing is valid if the wing mass is really small. Usually each wing accounts for 1% of the weight of the body. However the model used in this thesis, which is modeled after a hawkmoth

has total wing weight of $\sim 6\%$. The validity of this assumption will be checked in chapter 4. Model 2 derived gives the equations of motion of the body with wing inertia effect. i.e. the wing accelerations the body would feel. The last model is, the complete system, body and wings, the difference between model 2 and model 3 is that the wings are modeled as states in model 3 where as in model 2 the kinematics of the wings have been captured. The validity of each model will be checked in the next few chapters.

Chapter 3

THE AVERAGED NON-LINEAR MODEL

3.1 Introduction

As discussed previously, there are two ways of handling a time varying system, one is to use *Floquet theory* and the other is to use averaging theory, which is a perturbation method. In fact, Floquet theory converts time periodic vector field into an autonomous averaged form. Vela *et al.* (2002) demonstrates that averaging theory is a synthesis of Floquet theory and perturbation theory. In this thesis we have discussed averaging method, as applied to the MAV system. Since the idea of averaging is to get a time invariant model for control purposes, it is unsure how quarter cycle averaging proposed in Orlowski and Girard (2011a) is useful for purpose of control.

Averaging is a way to approximate behavior of a non-autonomous dynamical system 'on an average'. Simply put, a slow time varying system can be approximated by an averaged system, and the solution of the new averaged system is an average solution to the original system. Murdock (1999) and Sanders *et al.* (2007) are two good references for understanding of averaging theory. Averaging theory is applicable to a large class of time dependent vector field, not necessarily periodic. However the system under scrutiny is actuated by a periodic vector field. The motivation of averaging is that a physical system's response is determined more by the average influence rather than the fluctuations about the average. For averaging theory to be applicable it is necessary that the system is in *periodic standard form* (Murdock (1999)) i.e.

$$\dot{x} = \epsilon f(x, t, \epsilon), \quad x(0) = a \tag{3.1}$$

where f is 2π periodic in t. The necessity of this form, stems from the fact that averaging theory is only applicable when the system is varying *slowly*. Multiplying the right hand side by an ϵ term (where ϵ is tending to 0), makes the system evolve slowly, i.e. x is nearly a constant. And thus averaging this system makes sense. Example highlighting the significance of this will follow this discussion. First order averaging, the simplest form of averaging, entails replacing the above system by

$$\dot{z} = \epsilon \bar{f}(z), \quad y(0) = a \tag{3.2}$$

where,

$$\bar{f}(z) = \frac{1}{2\pi} \int_0^{2\pi} f(z, t, 0) dt \tag{3.3}$$

Introducing a new variable (or 'time scale') $\tau = \epsilon t$, removes the ϵ, results in *guiding system*

$$\frac{dw}{d\tau} = \bar{f}(w), \quad w(0) = a \tag{3.4}$$

The idea is, that the solution of the averaged system remains close to the solution of the original system, the error in this case is $\mathcal{O}(\epsilon)$ and the approximation is valid on a time interval $\mathcal{O}(t/\epsilon)$. In order to quantify this, the theorems below from Murdock (1999) are referred.

Theorem 3.1.1 *Assume 3.1 is smooth and periodic in t. Suppose 3.4 has a solution* $w(\tau, a)$ *which exists on the interval* $0 \leq \tau \leq T$. *Then there exist constants* $\epsilon_1 > 0$ *and* $c > 0$ *such that the solution of the exact system 3.1 exists on the expanding interval* $0 \leq \tau \leq \frac{T}{\epsilon}$, *and the following error estimate holds*
$\|x(t, a, \epsilon) - w(\epsilon t, a)\| < c\epsilon \quad for \quad 0 \leq t \leq T/\epsilon, \quad 0 \leq \epsilon \leq \epsilon_1$

The following example from Murdock (1999) shows the necessity of having small

termeϵ multiplying the right hand side of the ode.

$$\dot{x_1} = 1, \;\; x_1(0) = 0$$
$$\dot{x_2} = \epsilon \cos(x_1 - t), \;\; x_2(0) = 0 \tag{3.5}$$

The exact solution is $x_1 = t$ and $x_2 = \epsilon t$. However, if averaging were to be directly applied to the system, it would result into

$$\dot{z_1} = 1, \;\; z_1(0) = 0$$
$$\dot{z_2} = 0, \;\; z_2(0) = 0 \tag{3.6}$$

The exact solution to the averaged solution is $z_1 = t$ and $z_2 = 0$. The error in the second state equals 1 when $t = 1/\epsilon$. The error stems from the fact that, the first state evolves in a way, that the second state stays at its maximum, and thus is not represented correctly by its average value 0. If $\dot{x_1}$ were to be ϵ (periodic standard form) instead of 1, x_1 would have grown slowly over one time period and the cos term would perform a sinusoid and better approximated by its average 0.

In the next theorem from Murdock (1999), existence and stability of solution of the averaged system has been analyzed. The exact solution of the original system, tends to make small oscillations around a slowly moving guiding center, possibly drifting away from the center after a long duration, however at an equilibrium (if one exists) of the averaged system, the guiding center does not move and the solution of the exact system oscillates about this point.

Theorem 3.1.2 *Suppose that the system 3.1 is smooth and 2π periodic. Let the first order averaged 3.2 system have an equilibrium point $z = z_0$, that is $\bar{f}(z_0) = 0$, and let the matrix of the partial derivatives of $\bar{f}$ at this rest point be denoted by $A = \bar{f}(z_0)$. If A is nonsingular (then there exists a unique ϵ dependent initial condition $a(\epsilon)$, defined for ϵ in some interval $\|\epsilon\| < \epsilon_1$, such that $a(0) = z_0$ and such that the solution*

$x(t, a(\epsilon), \epsilon)$ of 3.1 with this initial condition is periodic with period 2π.

If the eigenvalues of A lie in the left half of the complex plane then the periodic solution $x(t, a(\epsilon), \epsilon)$ is asymptotically stable (all nearby solutions remain close to, and approach, the periodic solution as $t \to \infty$. If at least one eigenvalue lies in the right half-plane the periodic solution is unstable. If some eigenvalues are on the imaginary axis and the rest are in the left half plane, no conclusion about the stability of the periodic solution is possible from the first order averaged equation alone. In the first case (eigenvalues in the left half-plane), the basic error estimate $\|x - z\| < c\epsilon$ holds for all future time ($t > 0$, and not merely $0 < t < T/\epsilon$) for any solution that is attracted to the periodic solution as $t \to \infty$.

3.1.1 Averaging Method as Applied to the MAV System

The MAV system 2.6 has the following form:

$$\frac{dx}{dt} = f(x) + F(x, t) \tag{3.7}$$

To get it into standard periodic form, a fast variable τ is introduced as $\tau = t/\epsilon$. Thus $\dfrac{d\tau}{dt} = 1/\epsilon$, equation 3.7 changes to

$$\frac{dx}{d\tau} = \epsilon[f(x) + F(x, \tau)] \tag{3.8}$$

In the MAV system $1/\omega$ plays the role of ϵ. Based on the above theorem, the time varying system 3.7 can be approximated as time invariant averaged system, by averaging over one wing beat cycle ($\tau = \omega T = 2\pi$) as follows

$$\frac{d\bar{x}}{d\tau} = \epsilon f(\bar{x}) + \epsilon \frac{1}{T} \int_0^T F(t, x)dt \tag{3.9}$$

Changing the time scale back to t by we get,

$$\frac{d\bar{x}}{dt} = f(\bar{x}) + \frac{1}{T} \int_0^T F(t, x)dt \tag{3.10}$$

Averaging the system 2.6, we get the following

$$\begin{aligned}
\dot{\bar{u}} &= \frac{\bar{F}_x}{M_b} - g\sin\bar{\theta} - \bar{q}\bar{w} \\
\dot{\bar{w}} &= \frac{\bar{F}_z}{M_b} + g\cos\bar{\theta} + \bar{q}\bar{u} \\
\dot{\bar{\theta}} &= \bar{q} \\
\dot{\bar{q}} &= \frac{\bar{M}_y}{I_{yy}}
\end{aligned} \tag{3.11}$$

where,

$$\bar{F}_i = \frac{1}{2\pi}\int_0^{2\pi} F(t,x)_i dt$$

and similarly for the moment expression.

Using the same approach, averaging the system 3.12, we get the following

$$\begin{bmatrix} M_t & 0 & 0 & \overline{m14} \\ 0 & M_t & 0 & \overline{m24} \\ 0 & 0 & 1 & 0 \\ \overline{m14} & \overline{m24} & 0 & \overline{m44} \end{bmatrix} \begin{bmatrix} \dot{\bar{u}} \\ \dot{\bar{w}} \\ \dot{\bar{\theta}} \\ \dot{\bar{q}} \end{bmatrix} =$$

$$F = \begin{bmatrix} \bar{F}_x - M_t g\sin\bar{\theta} - M_t\bar{q}\bar{w} \\ -M_w(\bar{q}^2\frac{b_w}{2}\cos\beta\overline{\sin\phi} - \bar{q}^2 l_1 + 2\bar{q}\frac{b_w}{2}\sin\beta\overline{\dot{\phi}\cos\phi} + \frac{b_w}{2}\cos\beta\overline{\dot{\phi}^2\sin\phi}) \\ \bar{F}_z + M_t g\cos\bar{\theta} + M_t\bar{q}\bar{u} \\ -M_w(-\bar{q}^2\frac{b_w}{2}\sin\beta\overline{\sin\phi} + 2\bar{q}\frac{b_w}{2}\cos\beta\overline{\dot{\phi}\cos\phi} - \frac{b_w}{2}\sin\beta\overline{\dot{\phi}^2\sin\phi}) \\ \bar{q} \\ \bar{M}_y - M_w(\bar{q}\bar{w}\frac{b_w}{2}\sin\beta\overline{\sin\phi} - \bar{q}\bar{u}(l_1 - \frac{b_w}{2}\cos\beta\overline{\sin\phi}) \\ +\frac{b_w}{2}l_1\sin\beta\overline{\dot{\phi}^2\sin\phi} - 2\frac{b_w}{2}l_1\cos\beta\overline{\dot{\phi}\cos\phi} + g\sin\bar{\theta}\frac{b_w}{2}\sin\beta\overline{\sin\phi} \\ -g\cos\bar{\theta}\frac{b_w}{2}\cos\beta\overline{\sin\phi}) - I_{wx}(2\bar{q}\overline{\dot{\phi}\sin\phi\cos\phi}\cos^2\alpha \\ -\overline{\dot{\phi}^2\cos\phi}\sin\alpha\cos\alpha - I_{wy}(-2\bar{q}\overline{\dot{\phi}\sin\phi\cos\phi} - \dot{\alpha}\overline{\dot{\phi}\sin\phi}) \\ -I_{wz}(2\bar{q}\overline{\dot{\phi}\sin\phi\cos\phi}\sin^2\alpha - \overline{\dot{\phi}^2\cos\phi}\sin\alpha\cos\alpha \end{bmatrix} \tag{3.12}$$

This completes the discussion on first order averaging, which has been the most widely used method to deal with time variance of the system of differential equations in MAV research. However Taha *et al.* (2012) have claimed that first order averaging fails for the MAV system based on a Hawkmoth model because the $\epsilon = 1/\omega$ is not small enough. Thus, higher order averaging is required to get the right approximation of the original system. They use second order averaging and showed that the hover equilibrium changed. In the next section, we give a short introduction to second order averaging and apply it to the MAV model, used in this thesis, to check if second order averaging is indeed required.

3.2 Second Order Averaging

Higher order averaging is used to get better approximation of the time variant system. The purpose is twofold, first to get higher orders of accuracy on expanding intervals of length $\mathcal{O}(1/\epsilon)$; but in practice this is limited by the difficulty in computation, second, to extend the asymptotic length of the expanding intervals of validity. Besides these, higher order averaging is needed to determine stability of some periodic solutions which do not follow the rules of theorem 3.1.1 i.e. when the eigenvalues are on the imaginary axis.

We refer to the following theorem from Sanders *et al.* (2007). Starting with the system

$$\dot{x} = \epsilon f_1(x,t) + ... + \epsilon^k f_k(x,t) \tag{3.13}$$

with a period T in t.

If y represents the averaged variable x ($\bar{x}$), then the second order averaged system is given by

$$\dot{y} = \epsilon g_1 + ... + \epsilon^k g_k(y) \tag{3.14}$$

where

$$g_1 = \frac{1}{T}\int_0^T f_1(x,t)dt \tag{3.15}$$

$$g_2 = \frac{1}{T}\int_0^T (f_2 + D_y f_1(y,t)u_1(y,t) - D_y u_1(y,t)g_1(y))dt \tag{3.16}$$

$$u_1 = \int_0^t (f_1(y,\tau) - g_1(y))d\tau + c_1(y) \tag{3.17}$$

D_y represents the partial derivaive of the vector field w.r.t y.

c_1 here is taken as 0, as per *stroboscopic averaging* (for detailed explanation refer Murdock (1999))

An alternate expression of g_2 is presented in Vela *et al.* (2002)

$$g_2 = \frac{1}{2T}\int_0^T \left[\int_0^t f_1(x,\tau)d\tau, f_1(x,t)\right]dt \tag{3.18}$$

where [,] is a lie bracket. Then the solution of the original system is

$$\xi = y + \epsilon u_1(y,t) + ...\epsilon^{k-1}u_{k-1}(y,t) \tag{3.19}$$

The next theorem (Sanders *et al.* (2007))relates the two solutions, averaged and original.

Theorem 3.2.1 *The exact solution* $x(a,t,\epsilon)$ *and* $\xi(a,t,\epsilon)$ *are related by*

$\|x(t,a,\epsilon) - \xi(a,t,\epsilon)\| < \mathcal{O}(\epsilon^k)$

for time $\mathcal{O}(1/\epsilon)$

The improvement is of order ϵ^2. However this improvement in accuracy when traded off with the computational effort, is extremely small, as will be seen in the next section. Since calculating even the second order averaging terms, numerically is expensive, we have second order averaged only model 1 i.e. the body dynamics without any wing effects.

3.2.1 Second Order Averaging as Applied to the MAV System

The MAV system can be expressed as

$$\dot{x} = f(x, t, \epsilon) \tag{3.20}$$

This can be expanded in an ϵ series that looks like 3.13. However, we are interested in terms up to second order. System 3.7 when second order averaged takes the following form

$$\frac{dx}{dt} = \epsilon\big(\frac{1}{T}\int_0^T f(x) + F(x,t)\,dt\big) + \epsilon^2\big(\frac{1}{2T}\int_0^T \Big[\int_0^t F(x,\tau) + f(x)\,d\tau, \\ F(x,t) + f(x)\Big]\big) \tag{3.21}$$

The above equation is nothing but system 3.11 but with additional terms, corresponding to the integral given in equation 3.18.

$$\begin{aligned}
\dot{\bar{u}} &= \frac{\bar{F}_{1,x}}{M_b} + \frac{\bar{F}_{2,x}}{M_b} - g\sin\bar{\theta} - \bar{q}\bar{w} \\
\dot{\bar{w}} &= \frac{\bar{F}_{1,z}}{M_b} + \frac{\bar{F}_{2,z}}{M_b} + g\cos\bar{\theta} + \bar{q}\bar{u} \\
\dot{\bar{\theta}} &= \bar{q} \\
\dot{\bar{q}} &= \frac{\bar{M}_{1,y}}{I_{yy}} + \frac{\bar{M}_{2,y}}{I_{yy}}
\end{aligned} \tag{3.22}$$

where F_1 and F_2 are given in equations 3.15 and 3.16. The second order averaged expressions of the terms that are functions of only the states, cancel each other out; and only first order averaged states remain.

After obtaining the averaged system, the next step is linearization. The operating point about which the model is linearized and the linear model will be shown in detail in the next chapter. For the sake of comparison of first and second order averaging,

Table 3.1: Open Loop Eigenvalues of Linear Model Based on First Order Averaging

Pole	Damping	ω_n
-6.74	1	6.74
-12.5	1	12.5
4.73 + j9.81	-0.434	10.9
4.73 - j9.81	-0.434	10.9

Table 3.2: Open Loop Eigenvalues of Linear Model Based on Second Order Averaging

Pole	Damping	ω_n
-6.89	1	6.89
-14.1	1	14.1
3.27 + j9.67	-0.321	10.2
3.27 - j9.67	-0.321	10.2

we go ahead of the flow of discussion and present the eigenvalues of the linear map. All computations have carried out numerically.

As clearly seen from the tables the difference between the eigenvalues is not much. We expect the difference to be small because the change should be on the order ϵ^2. We conclude that the stability properties remained the same after second order averaging.

3.3 Summary

In this chapter we reviewed averaging concepts, first order averaging is almost universally used for the analysis of flapping wing MAVs. The theory of averaging basically predicts the averaged behavior of the sysetm, which is under the influence

of a time varying vector field. It approximates the solution of the original non-autonomous system. The concept of higher order averaging was introduced here, to analyze if we could obtain a better approximation of the periodic nonlinear model. However the linearizations based on both first and second order averaging were found to be very close to each other. We conclude that the need for higher order averaging at least for the model used here doesn't seem necessary. As will be seen in the next 2 chapters, feedback control based on first order averaging is able to stabilize the nonlinear model quite well.

Chapter 4

THE LINEAR TIME INVARIANT MODEL AND TRADE-STUDIES

The full 6 DOF nonlinear model for both, with and without wings were developed in chapter 2. In chapter 3 averaging theory and analysis of time varying systems were discussed. The system in question is actuated by a periodic vector field and hence belongs to this class of systems. In this chapter, the averaged nonlinear system is linearized about *hover* equilibrium and analysis of the linear model follows for both model 1 (body without wing inertial effect) and model 2 (body with wing inertial effect). The average model was derived in section 3.1.1 To be able to stabilize the model at hover, the equilibrium parameters need to be evaluated. It is important to see that there is no equilibrium point for the system 2.6; as the wings go back and forth, the body too oscillates, thus we are looking for a periodic trajectory that stabilizes the insect about the desired equilibrium point. But this point serves as an equilibrium for the averaged system, about which it is linearized. The questions that are of interest here, are

1. When does averaging work/not work?
2. What closed loop bandwidth must be sufficiently small?
3. When is lower order averaging sufficient?

4.1 Analysis of Linear Model 1: Body Without Wing Inertial Effect

The equilibrium for the averaged system is found using Matlab's *fmincon* command. Sum of squares of all state derivatives was minimized. Because of hover flight

condition, this corresponds to zero, translational and angular velocities. The table below gives all the parameters and state values at equilibrium. For convenience, meaning of the variables is restated

u, w	Body velocities in x_b and z_b axis
θ	Body pitch angle
q	Body angular velocity in y_b axis
ω	Wing flapping frequency
β	Stroke plane angle
ϕ, ϕ_0	Flapping amplitude and offset
α, α_0	Pitch amplitude and offset

Table 4.1: Hover Parameters

u (m/s)	w (m/s)	θ°	q (rad/s)	ω (Hz)	β°	ϕ°	ϕ_o°	α°	α_o°
0	0	90	0	30	-90	50	0	25.219	0

Let X, Z be the components of F_a along the x_b, z_b direction respectively, and M be the y_b component of the M_a. These forces and moments are cycle averaged and functions of states $\mathbf{x} = [u \ w \ \theta \ q]$ and wing stroke parameters $\mathbf{p} = [\omega \ \beta \ \phi_m \ \phi_o \ \alpha_m \ \alpha_o]$. If each variable is expressed as a sum of equilibrium state and a perturbation,

$$\mathbf{x} = \mathbf{x}_e + \delta\mathbf{x}, \quad \mathbf{p} = \mathbf{p}_e + \delta\mathbf{p}$$
$$\mathbf{X} = \mathbf{X}_e + \delta\mathbf{X} \tag{4.1}$$

The linearized equations can be written as:

$$\delta\dot{u} = \frac{\delta X}{M_b} - g\cos\delta\theta \tag{4.2}$$

$$\delta\dot{w} = \frac{\delta Z}{M_b} - g\sin\delta\theta \tag{4.3}$$

$$\delta\dot{\theta} = \delta q \tag{4.4}$$

$$\delta\dot{q} = \frac{\delta M}{I_b} \tag{4.5}$$

The perturbations in the aerodynamic forces and moments are expressed as

$$\delta X = X_u\delta u + X_w\delta w + X_q\delta q + X_\omega\delta\omega + X_\beta\delta\beta + X_{\phi_m}\delta\phi_m + X_{\phi_o}\delta\phi_o + X_{\alpha_m}\delta\alpha_m + X_{\alpha_o}\delta\alpha_o \tag{4.6}$$

δZ and δM are similarly expressed as summation of partial derivatives. These derivative terms w.r.t to the body velocities are called stability derivatives and the derivatives w.r.t the wing parameters are called control derivatives.

4.1.1 Choice of Controls

To decide between control and fixed parameters, and the optimum number of controls required, the jacobian of the forces $[X, Z, M]$ w.r.t the wing stroke parameters is examined. This helps in checking the relative importance of each parameter. A similar procedure is taken by Karásek and Preumont (2012). Recognizing that the vehicle can be controlled by, frequency (ω), stroke plane angle (β), flapping parameters (ϕ, ϕ_o) and lastly pitching parameters (α, α_o) only, we obtain the following system 'B' matrix

$$\begin{bmatrix} 0.0018 & 0 & 0.2626 & 0 & 0.2102 & 0 \\ -0.0007 & -0.1146 & 0 & 0 & 0 & -0.155 \\ 0 & 0 & 0 & 0 & 0 & 0 \\ 0.0039 & -0 & 0 & -1.7164 & 0 & 0.709 \end{bmatrix} \tag{4.7}$$

It is seen from above, that the parameters that affect the force in x_b direction/lift direction and moment along y_b are α_m, ϕ_m and the parameters affecting the force in z_b direction/drag direction are β, α_o and ϕ_o. It follows that the vertical dynamics is decoupled from the horizontal and pitch dynamics. this decoupling is characteristic of hover and as seen later, in forward flight this will not hold true anymore. A point to note here is that the body x_b direction is along the longitudinal axis, which is perpendicular to the inertial x_e axis, and the body's z_b is along the x_e and hence the swap seen in the rows of B matrix. The first row corresponds to vertical dynamics and second tow corresponds to horizontal dynamics.

For controlling the flight $[\phi_o, \alpha_m, \alpha_o]$ are chosen as control parameters. Since the system is decoupled, α_m is to chosen to control the vertical force and ϕ_o, α_o are chosen to control force and moment in horizontal and pitch direction. An SVD further shows the relative importance of these control parameters on the states. Humbert and Faruque (2011) perform a reachability analysis with chosen control parameters to choose the optimum combination. To further support this decision we use the figure 2.1, the significance of differential angle of attack can be appreciated. Thrust is generated in upstroke and the magnitude is directly proportional to the angle of attack, thus the angle of attack should be higher in the upstroke than in the downstroke. Hence the differential angle of attack is responsible for thrust and an essential control parameter in forward flight. α_m is $(\alpha_u + \alpha_d)/2$. Amplitude offset is directly tied with the pitch, if the flap is made ahead of the body/in front of the C.G, it provides a CW moment and vice versa.

The LTI model can be represented in state space as

$$\dot{x} = Ax + Bu$$

$$y = Cx + Du$$

$$A = \begin{bmatrix} -6.741 & 0 & 0 & -0.076 \\ 0 & -2.772 & -9.81 & 0.005 \\ 0 & 0 & 0 & 1 \\ 0 & 151.611 & 0 & -0.308 \end{bmatrix}, \quad B = \begin{bmatrix} 0 & 18 & 0 \\ 0 & 0 & -13.3 \\ 0 & 0 & 0 \\ 1544 & 0 & 638 \end{bmatrix}$$

$$C = \begin{bmatrix} 1 & 0 & 0 & 0 \\ 0 & 1 & 0 & 0 \\ 0 & 0 & 1 & 0 \end{bmatrix}, \quad D = \begin{bmatrix} 0 & 0 & 0 \\ 0 & 0 & 0 \\ 0 & 0 & 0 \end{bmatrix} \tag{4.8}$$

The outputs are $[u, w, \theta]$. With these as the outputs, the flight path angle and the total forward velocity can by computed.

The Eigenvalues, with their corresponding damping ratio and natural frequency are as given below. The open loop plant has no transmission zeros.

Table 4.2: Plant Eigenvalues

Pole	Damping	ω_n
-6.74	1	6.74
-12.5	1	12.5
4.73 + j9.81	-0.434	10.9
4.73 - j9.81	-0.434	10.9

Hover is thus an unstable equilibrium. Active control is required to maintain hover. Since the instability is at roughly at 11 rad/s, we expect the minimum input bandwidth to be at least twice this figure.

4.1.2 SVD Analysis

A singular value decomposition at DC yields the following:

$$\begin{aligned} G(j0) &= C(A)^{-1}B + D \\ &= U\Sigma V^T \end{aligned} \tag{4.9}$$

$$U = \begin{bmatrix} 0 & -1 & 0 \\ -0.9727 & 0 & -0.2321 \\ 0.2321 & 0 & -0.9727 \end{bmatrix}, \quad \Sigma = \begin{bmatrix} 11.33 & 0 & 0 \\ 0 & 2.67 & 0 \\ 0 & 0 & 1.21 \\ 0 & 0 & 0 \end{bmatrix}$$

$$V = \begin{bmatrix} -0.9337 & 0 & 0.3580 \\ 0 & -1 & 0 \\ 0.3580 & 0 & 0.9337 \end{bmatrix} \tag{4.10}$$

The SVD at hover clearly shows the decoupling between input u_2 to output y_1 and inputs u_1, u_3 to outputs y_2 and y_3. Also note that u_1 has a major contribution towards y_2 and u_3 contributes more to y_3. This is in accordance with the force resolution discussion before, pitch angle magnitude (α_m) is responsible for lift hence the vertical dynamics (along x_b), while the pith offset (ϕ_o) is responsible for moment, hence body pitch and lastly pitch offset α_o is responsible for the horizontal dynamics, (along z_b).

To emphasize that decoupling of controls is only true at hover, SVD analysis at other flight speeds (all at D.C) is checked.

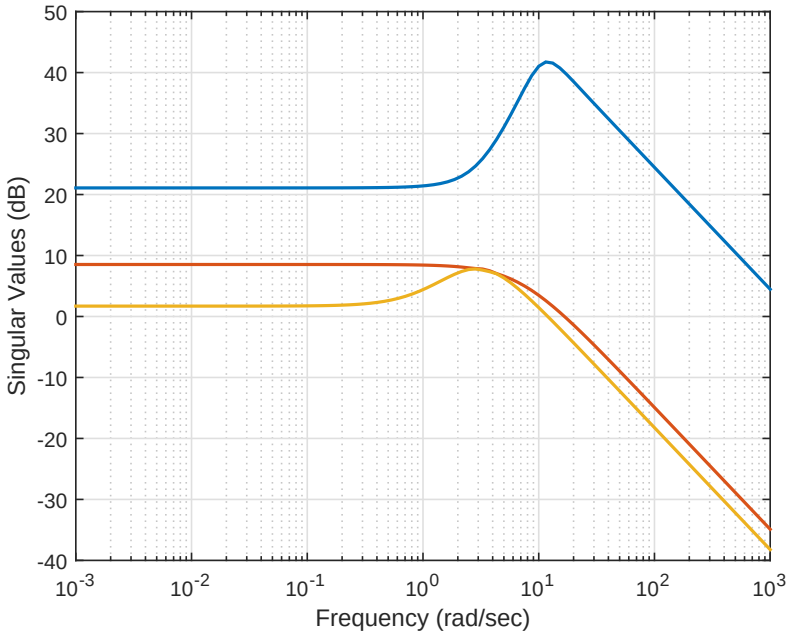

Figure 4.1: SVD at Hover

Singular value decomposition at 0.5 m/s

$$U = \begin{bmatrix} -0.4292 & 0.6131 & 0.6632 & 0 \\ -0.8306 & -0.5564 & -0.2321 & 0 \\ 0.3549 & -0.5608 & 0.7481 & 0 \\ 0 & 0 & 0 & 1 \end{bmatrix}, \quad \Sigma = \begin{bmatrix} 10.869 & 0 & 0 \\ 0 & 2.347 & 0 \\ 0 & 0 & 1.407 \\ 0 & 0 & 0 \end{bmatrix}$$

$$V = \begin{bmatrix} -0.9773 & 0.1538 & -0.1454 \\ 0.0117 & 0.7251 & 0.6885 \\ 0.2114 & 0.6712 & -0.7105 \end{bmatrix} \tag{4.11}$$

Singular value decomposition at 1.0 m/s

$$U = \begin{bmatrix} -0.8917 & 0.0785 & 0.4458 & 0 \\ -0.2247 & -0.9317 & -0.2853 & 0 \\ 0.3930 & -0.3546 & 0.8484 & 0 \\ 0 & 0 & 0 & 1 \end{bmatrix}, \quad \Sigma = \begin{bmatrix} 10.495 & 0 & 0 \\ 0 & 3.727 & 0 \\ 0 & 0 & 0.7048 \\ 0 & 0 & 0 \end{bmatrix}$$
$$V = \begin{bmatrix} -0.9899 & 0.1386 & -0.0295 \\ 0.0560 & 0.5734 & 0.8174 \\ 0.1302 & 0.8075 & -0.5753 \end{bmatrix} \tag{4.12}$$

Singular value decomposition at 1.5 m/s

$$U = \begin{bmatrix} -0.9568 & -0.0269 & 0.2895 & 0 \\ -0.0438 & -0.9710 & -0.2350 & 0 \\ 0.2874 & -0.2375 & -0.9279 & 0 \\ 0 & 0 & 0 & 1 \end{bmatrix}, \quad \Sigma = \begin{bmatrix} 9.481 & 0 & 0 \\ 0 & 4.363 & 0 \\ 0 & 0 & 0.689 \\ 0 & 0 & 0 \end{bmatrix}$$
$$V = \begin{bmatrix} -0.9639 & 0.1944 & -0.1818 \\ 0.0219 & 0.7387 & 0.6737 \\ 0.2652 & 0.6454 & -0.7164 \end{bmatrix} \tag{4.13}$$

Singular value decomposition at 2.0 m/s

$$U = \begin{bmatrix} -0.9214 & -0.2830 & 0.2664 & 0 \\ 0.2245 & -0.9471 & -0.2295 & 0 \\ 0.3172 & -0.1517 & 0.9361 & 0 \\ 0 & 0 & 0 & 1 \end{bmatrix}, \quad \Sigma = \begin{bmatrix} 14.525 & 0 & 0 \\ 0 & 4.212 & 0 \\ 0 & 0 & 0.046 \\ 0 & 0 & 0 \end{bmatrix}$$
$$V = \begin{bmatrix} -0.9933 & -0.1159 & -0.004 \\ -0.0647 & 0.5259 & 0.8481 \\ -0.0962 & 0.8426 & -0.5298 \end{bmatrix} \tag{4.14}$$

The 'U' matrix at hover clearly shows decoupling between u, θ and w states, and as the forward speed increases this ceases to be true.

4.2 Analysis of Linear Model 2: Body with Wing Inertial Effect

The equilibrium at hover corresponds to the parameters shown in table 4.3

Table 4.3: Hover Parameters

u (m/s)	w (m/s)	θ°	q (rad/s)	ω (Hz)	β°	ϕ°	ϕ_o°	α°	α_o°
0	0	90	0	30	-90	50	0	27.17	0

The only change is in the magnitude of the angle of attack, which went up by almost 2°. The LTI model is represented in state space as

$$\dot{x} = Ax + Bu$$

$$y = Cx + Du$$

$$A = \begin{bmatrix} -5.886 & 0 & 0 & -0.064 \\ 0 & -2.831 & -9.81 & 0.006 \\ 0 & 0 & 0 & 1 \\ 0 & 151.753 & 0 & -0.328 \end{bmatrix}, B = \begin{bmatrix} 0 & 15.3 & 0 \\ 0 & 0 & -13.7 \\ 0 & 0 & 0 \\ -1337.7 & 0 & 547.4 \end{bmatrix}$$

$$C = \begin{bmatrix} 1 & 0 & 0 & 0 \\ 0 & 1 & 0 & 0 \\ 0 & 0 & 1 & 0 \end{bmatrix}, \quad D = \begin{bmatrix} 0 & 0 & 0 \\ 0 & 0 & 0 \\ 0 & 0 & 0 \end{bmatrix} \tag{4.15}$$

The Eigenvalues, with their corresponding damping ratio and natural frequency are as given below. The open loop plant has no transmission zeros.

Again, like in the previous case, the hover is an unstable equilibrium. The instability in this case too is at 11 rad/s, and we desire the bandwidth at the controls to be at least twice of this instability.

Table 4.4: Plant Eigenvalues

Pole	Damping	ω_n
-5.89	1	5.89
-12.6	1	12.6
4.71 + j9.81	-0.433	10.9
4.71 - j9.81	-0.433	10.9

Singular value decomposition at D.C gives the following

$$U = \begin{bmatrix} 0 & 1 & 0 & 0 \\ 0.9889 & 0 & -0.1485 & 0 \\ -0.1485 & 0 & -0.9889 & 0 \\ 0 & 0 & 0 & 1 \end{bmatrix}, \quad \Sigma = \begin{bmatrix} 6.6125 & 0 & 0 \\ 0 & 2.5969 & 0 \\ 0 & 0 & 1.0352 \\ 0 & 0 & 0 \end{bmatrix}$$
$$V = \begin{bmatrix} 0.7628 & 0 & 0.6466 \\ 0 & 1 & 0 \\ -0.6466 & 0 & 0.7628 \end{bmatrix} \tag{4.16}$$

A similar decoupling between input u_2 to output y_1 and input u_1, u_3 to output y_2 and y_3 is seen here. Thus, we see there is very little difference between the linear plants of both the models.

4.3 Trade Studies

In this section, we will discuss design aspects of the MAV, changing the geometric and mass properties to get suitable properties. Specifically, how the vehicle dimension l_1 (wing hinge distance from body C.G.) and the moment of inertia I_b affect the control of the MAV.

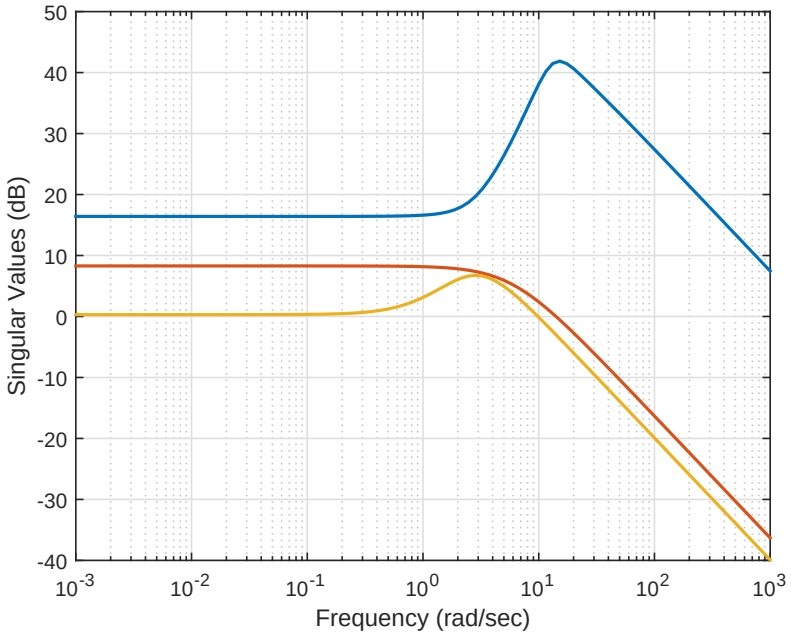

Figure 4.2: SVD at Hover

4.3.1 Effect of Wing Hinge Location

This dimension is directly related with pitch stability. Ideally for static stability the aerodynamic center of pressure should lie behind and/or below the center of gravity (Taylor and Thomas (2002)). However during flapping flight, the exact position of this aerodynamic center varies and difficult to locate. Ristroph *et al.* (2013) and Phan *et al.* (2012) discuss pitch stability in flapping insects. We vary the l_1 dimension to understand its significance. The moment produced by the wing, acts through this arm. Since for a stable configuration, the center of pressure should be typically below and behind the center of gravity, we expect the instability associated with pitch dynamics to decrease as we decrease this length.

To see the effect of the parameter l_1 we recalculate the eigenvalues, which will quantify the change in the stability property.

Comparing the eigenvalues with those listed in table 4.2, we notice that the in-

Table 4.5: Open Loop Eigenvalues for $l_1 = 120mm$

Pole	Damping	ω_n
-6.74	1	6.74
-18.4	1	18.4
5.27 + j12.9	-0.378	13.9
5.27 - j12.9	-0.378	13.9

stability has increased from 11 rad/s to 14 rad/s.

We are also interested in the maximum bandwidth at controls (input) that the system can handle. Higher bandwidth at the controls tends to destabilize the system. We expect this maximum limit can be pushed as this dimension tends to zero. The table below shows the maximum crossover frequency (approximate) beyond which the system destabilizes, the corresponding crossover frequency at the output, as the l_1 tends to zero. A point worth noticing here is, because this parameter is directly linked to the total moment at the C.G, we expect the amplitude of angular velocity 'q' about the mean to decrease simultaneously.

To elaborate on the point that the amplitude of angular velocity indeed decreases with a simultaneous decrease in the magnitude of l_1, the following time responses of q are presented. The procedure to obtain a stabilizing closed loop will be explained in the next chapter. The design shown below (figure 4.3) corresponds to input bandwidth close to 48 rad/s.

To conclude the distance to the wing hinge is an important dimension. It directly affects the stability and the amplitude of oscillations. Ideally we would like this dimension to be as small as possible. As mentioned before, one disadvantage is losing pitch control, which can be regained by having the wings flap asymmetrically about

Table 4.6: Effect of Decreasing l_1

Fraction of l_1	Input ω_c	Output ω_c	Maximum Amplitude of q (rad/s)
1	140	10	7
0.9	150	9.7	7
0.8	165	9.4	6
0.7	185	9	6
0.6	195	8.8	5
0.5	215	8.4	5
0.4	235	8.2	5.5
0.3	255	7.9	5.5
0.2	290	7.6	4
0.1	320	7.2	3.5
0	>350	<7	3.5

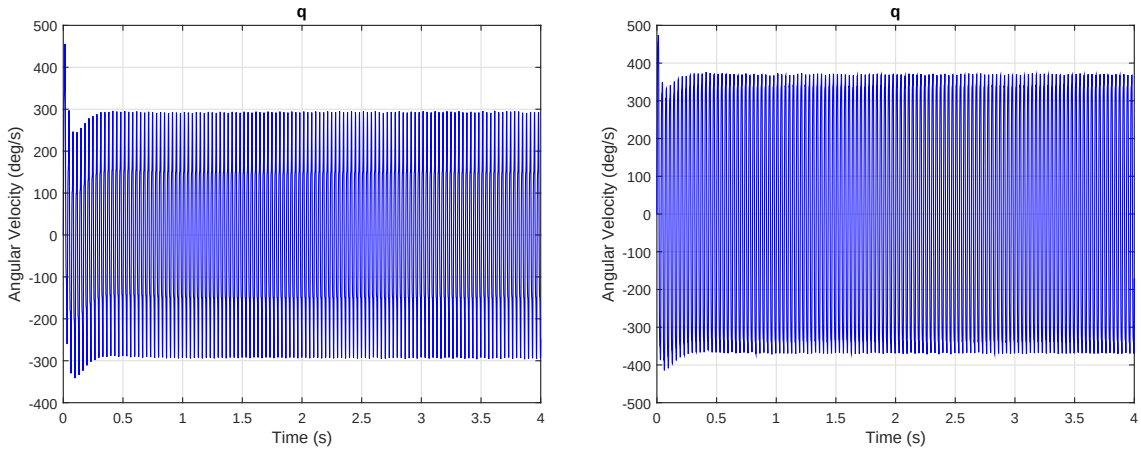

(a) With $l_1 = 0$

(b) With $l_1 = 120$ mm

Figure 4.3: Effect of Varying l_1 Dimension on Time Response of q

the out of plane axis i.e. to have offset in the flapping.

4.3.2 Effect of Moment of Inertia

The moment of inertia decides the pitch stability of the vehicle. In all of the time responses of q, the amplitude of oscillation is quite high (> 4 rad/s). This is attributed to the extremely low moment of inertia of the body. We expect that as the moment of inertia increases the instability associated with the pitch would decrease and the amplitude of pitch oscillation would become smaller.

The moment of inertia of the hawkmoth is on the order of 10^{-7}. The following table shows the effect of increasing moment of inertia from 10^{-7} to 10^{-4} on the unstable pole. The instability significantly decreases with an increase in the moment of inertia.

Table 4.7: Effect of Increasing I_{by}

Moment of Inertia	Unstable pole	Frequency
10^{-7}	$5.27 \pm$ j12.9	13.9
10^{-6}	$3.53 \pm$ j8.12	8.85
10^{-5}	$1.37 \pm$ j3.68	3.93
10^{-4}	$0.355 \pm$ j1.54	1.58

The oscillations of pitch velocity too decrease with the increase in the moment of inertia as evinced by the following plots (figure 4.4).

It is clear that as the moment of inertia decreases there is a drastic decrease in the amplitude of oscillations. We end the section by concluding that both moment of inertia and distance to the wing hinge are important parameters that significantly change the design of the system. Moment of inertia plays a major role in deciding

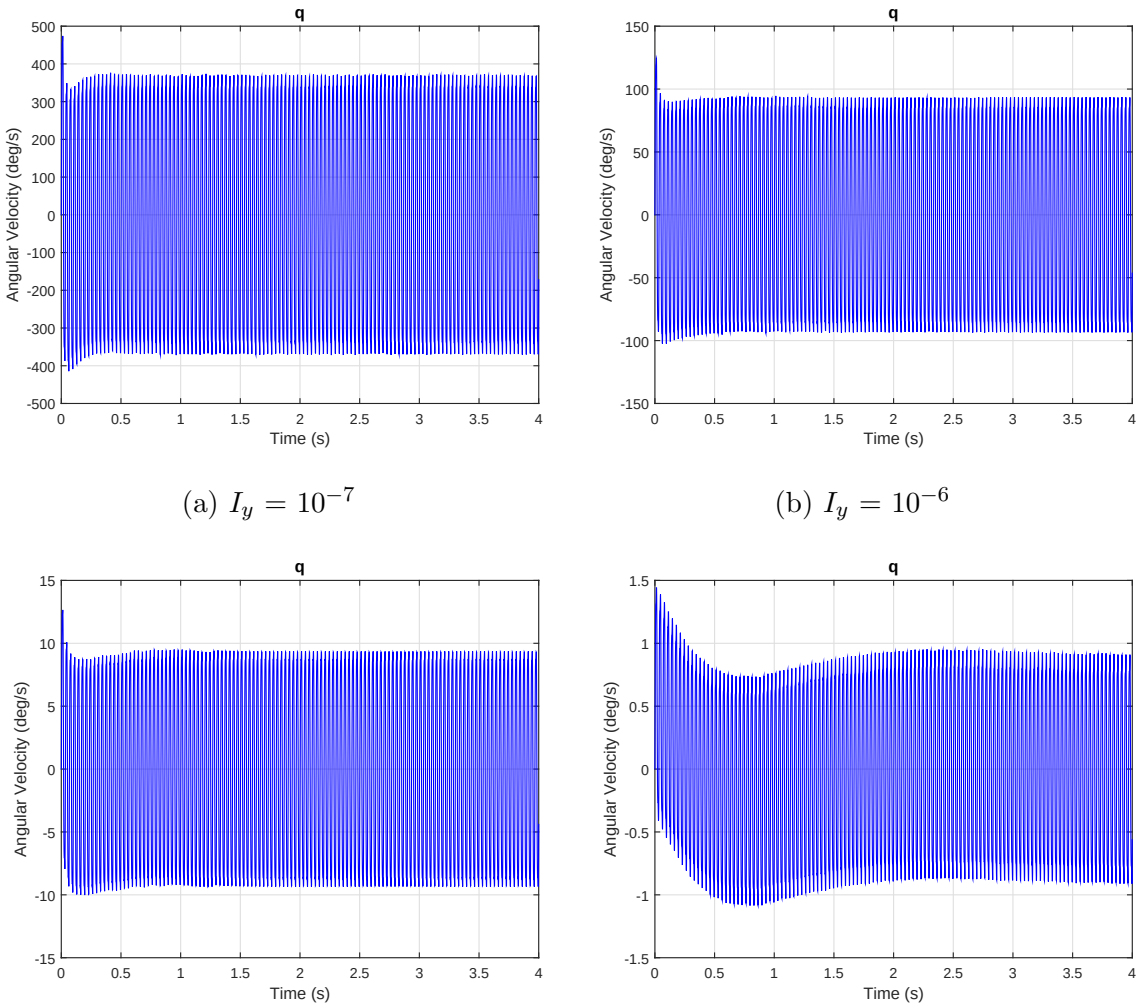

(a) $I_y = 10^{-7}$

(b) $I_y = 10^{-6}$

(c) $I_y = 10^{-5}$

(d) $I_y = 10^{-4}$

Figure 4.4: Effect of Varying Moment of Inertia on Time Response of q

the stability of the system. While deciding the geometry of the vehicle, we must try to maximize the rotational inertia and position the wing hinge as close as possible to the body C.G.

4.4 Summary

In this chapter we compared the two linear models corresponding to model 1(without wing inertial effect) and model 2 (body with wing inertial effect). We see the linear models are quite similar to each other. The linear model shows decoupling at D.C. It decouples into a SISO and two input two output system. Lastly design of the vehicle with respect to geometric parameters, wing hinge position and moment of inertia was discussed. It was noticed that both quantities have significant effect on body pitch amplitude and bandwidth at input.

Chapter 5

THE CONTROLLER DESIGN

In the literature of flapping wing MAV control, many different control schemes have been proposed. Classical PID control has been popular (Karásek and Preumont (2012)) with inner and outer loop which exploits the decoupled nature of hover, LQR has been used widely (Deng *et al.* (2006a)). A new robust control strategy has been adopted in Serrani *et al.* (2010) which is quite unique. Nonlinear control method has been used in Khan and Agrawal (2007). In this thesis we have opted for LQR methodology. In this chapter a linear controller for model 1 is designed and its performance is checked on the non-autonomous nonlinear system. Desired closed loop maps and the trade offs seen in controller performance are discussed. Later we discuss the effectiveness/robustness of this controller on the model with wing inertia. The gain matrices obtained in the previous designs is used to stabilize the second linear model. The same closed loop properties that were of interest in case one, are analyzed again. In section 3, we check up to what percentage, wing mass expressed as percentage of body weight, can the controller tolerate. In section 4, we design a controller for the model 2 and test it on the original model. The questions that are of interest are

1. Till what speed is nominal hover controller sufficient?
2. At what speed is a non-hover cruise controller necessary?
3. When is mass-less wing model sufficient?
4. When is wing mass necessary to model?

5. How much wing mass uncertainty can nominal hover controller tolerate?

6. When is a new controller necessary?

5.1 LQR Control

To stabilize the system at hover, full state feedback, linear, multivariable LQR was designed. LQR is formulated to minimize the following quadratic cost function

$$min_u \;\; J(u) = \frac{1}{2}\int_0^\infty x^\top(t)Qx(t) + u^\top(t)Ru(t)dt \tag{5.1}$$

where $Q \geq 0$ and $R > 0$ are the weighting matrices that trade off regulation performance and control effort. The structure chosen here was that of a *LQ servo loop* as shown in figure 5.1, the advantage is that, command following, disturbance and noise attenuation can be addressed directly. LQ servo augments the closed loop with integrators, hence zero steady state error to step response is possible.

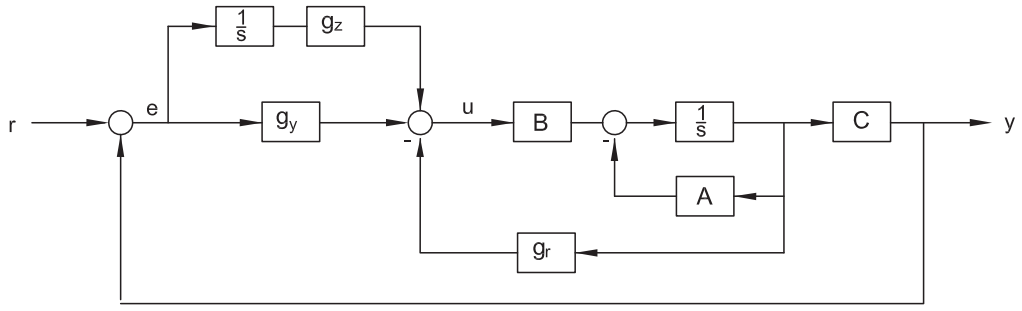

Figure 5.1: LQ Servo Loop

The controller was designed by iteratively tuning diagonal weighting matrices to ensure good closed loop properties. An optimization code (using MATLAB's *fmincon* function) was run to optimize minimum damping ratio and control bandwidth. We expect the minimum damping ratio to be no less that 0.5, ideally close to 0.707 and the bandwidth at the controls to be close to 22 rad/s (at least twice the instability

as mentioned before).

The other closed loop design objectives that are desired are

- $\sigma_{max}[S_o(j\omega)]$ and $\sigma_{max}[S_i(j\omega)]$ (i.e. Sensitivity at plant output and input) should be small at low frequencies for low frequency command following and disturbance attenuation.

- $\sigma_{max}[T_o(j\omega)]$ and $\sigma_{max}[T_i(j\omega)]$ (i.e.complementary sensitivity at plant output and input) should be small at high frequencies for high frequency noise attenuation.

- $\sigma_{max}[T_{ru}(j\omega)]$ (i.e. reference to control) should not be too large, it may result in unnecessarily large controls in the presence of typical reference commands.

- $\sigma_{max}[T_{diy}(j\omega)]$ (i.e. input disturbance to output) should be low at all frequencies for good low and high frequency disturbance attenuation.

Keeping the above points in mind, a series of controllers were designed where an acceptable trade off between minimum damping ratio (ζ), maximum settling time (T_s) and crossover frequency of L_u (loop broken at control input to plant) was achieved. Table 5.1 compares the maximum damping ratio, minimum settling time and the L_u crossover frequency (ω_c) for model 1 and model 2.

The figures 5.2 - 5.9 below show the closed loop performance corresponding to these designs. *The respective designs vary from light to dark shade of blue. The chosen design is in red.* The following is observed from the plots:

1. We desire a closed loop bandwidth at controls to be close to 22 rad/s, which would be at least twice the instability's frequency. However, to get a minimum desirable damping ratio (for good performance), a minimum of 32 rad/s ω_c is required.

Table 5.1: LQR Design Comparison

Min. ζ	Min. T_s	Lu ω_c	Min. ζ	Min. T_s	Lu ω_c
0.5132	3.144	32	0.4125	3.025	28
0.5962	3.117	38	0.5264	3.005	33.152
0.6254	3.11	42	0.5535	3.022	36.692
0.6133	3.10	48	0.5875	2.974	41.727
0.6131	3.093	52	0.5946	2.966	45.154

2. Closed loop properties get better with more bandwidth at controls.

3. The peaks of S_o and T_o are below 6 dB. Plots show that low frequency disturbance attenuation and high frequency noise attenuation will be achieved.

4. The peaks of S_i and T_i are below 0 and 6 dB respectively. But this is a property of LQR, it guarantees good properties at the plant input.

5. Peak of KS is mostly below 0 dB, which is desirable for not much control effort.

6. Peak of T_{diy} large, which is undesirable.

7. As T_o bandwidth increases, the closed loop properties get better, however the linear controller fails to stabilize the nonlinear plant. The maximum T_o bandwidth that could stabilize the nonlinear system was close to 30 rad/s. This is expected, because averaging is strictly possible if the bandwidth of the system is small enough to reject wing's high frequency input.

With this we have answered most of the questions posed in the beginning of the section. The answers will be summarized at the end again.

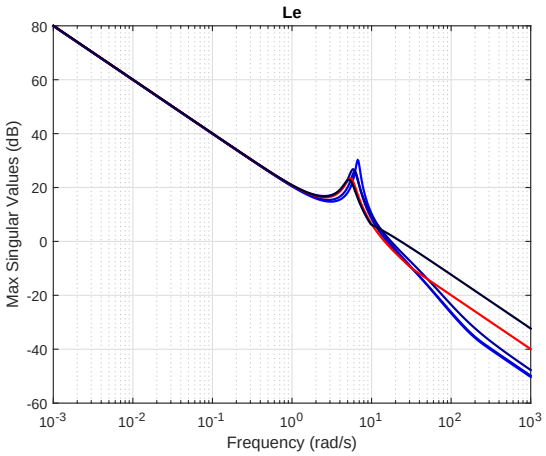

(a) Maximum Singular Value (Model 1)

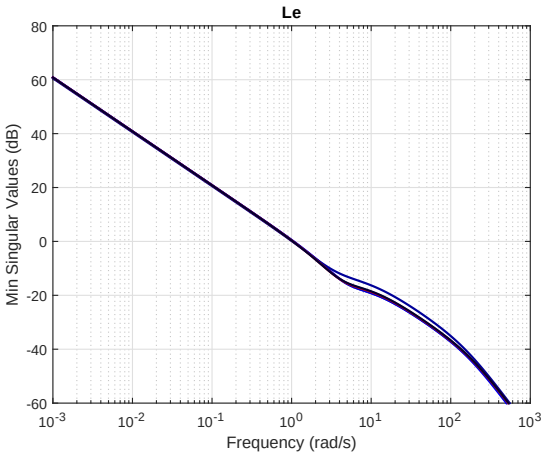

(b) Minimum Singular Value (Model 1)

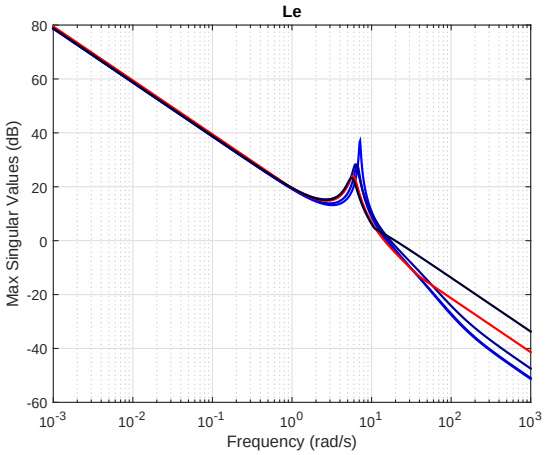

(c) Maximum Singular Value (Model 2)

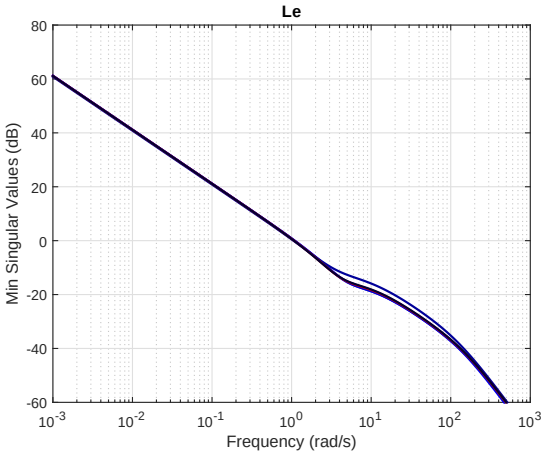

(d) Minimum Singular Value (Model 2)

Figure 5.2: Open Loop Map at Output; Designs vary from light to dark shade of blue; Chosen design is in red

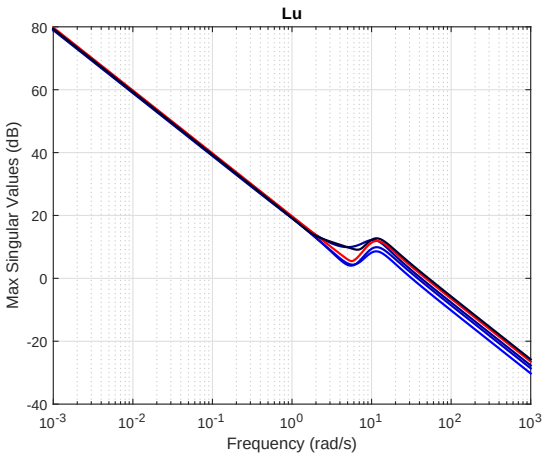

(a) Maximum Singular Value (Model 1)

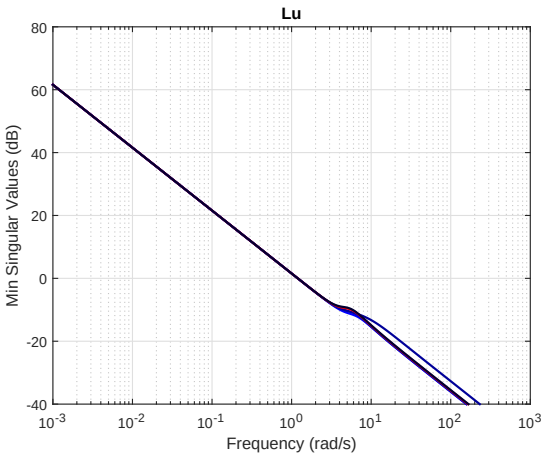

(b) Minimum Singular Value (Model 1)

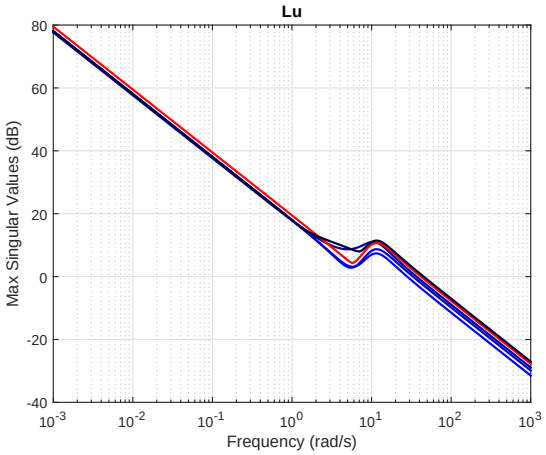

(c) Maximum Singular Value (Model 2)

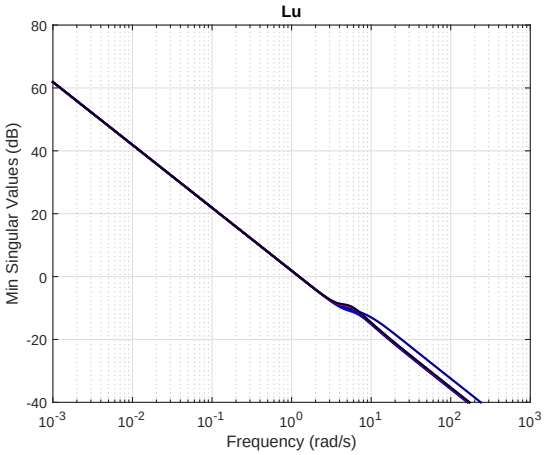

(d) Minimum Singular Value (Model 2)

Figure 5.3: Open Loop Map at Input

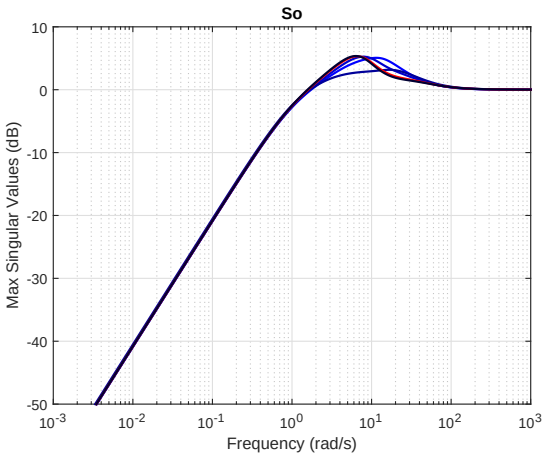

(a) Maximum Singular Value (Model 1)

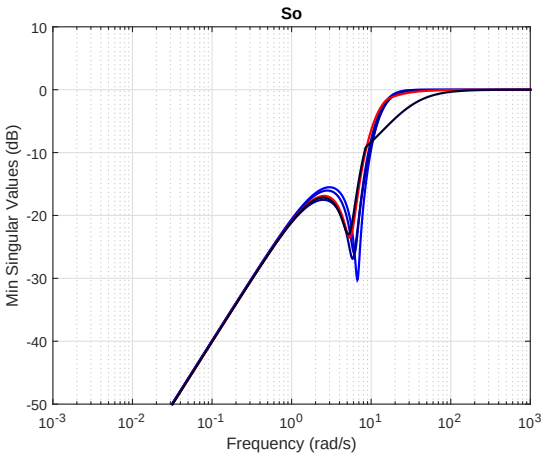

(b) Minimum Singular Value (Model 1)

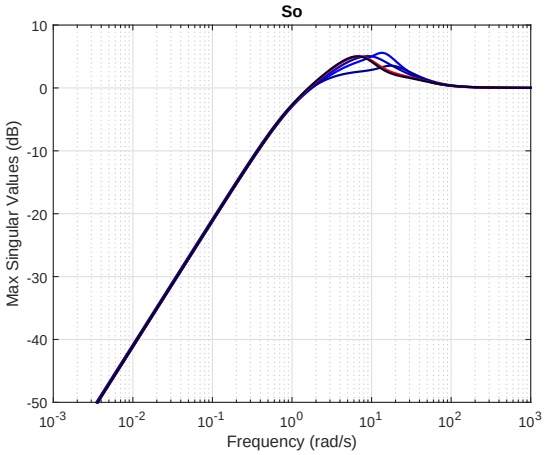

(c) Maximum Singular Value (Model 2)

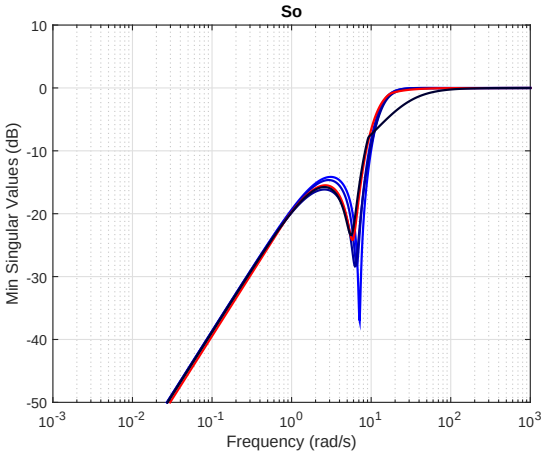

(d) Minimum Singular Value (Model 2)

Figure 5.4: Sensitivity at Output

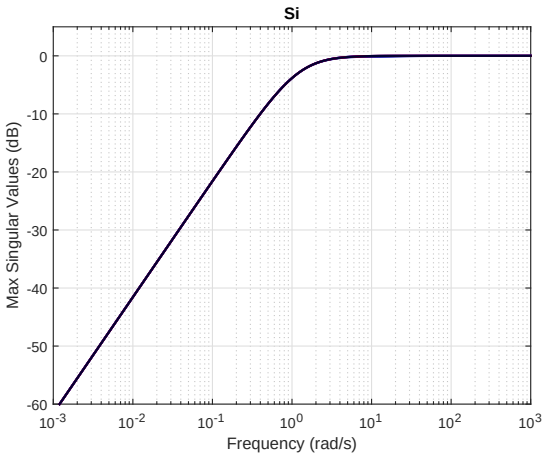

(a) Maximum Singular Value (Model 1)

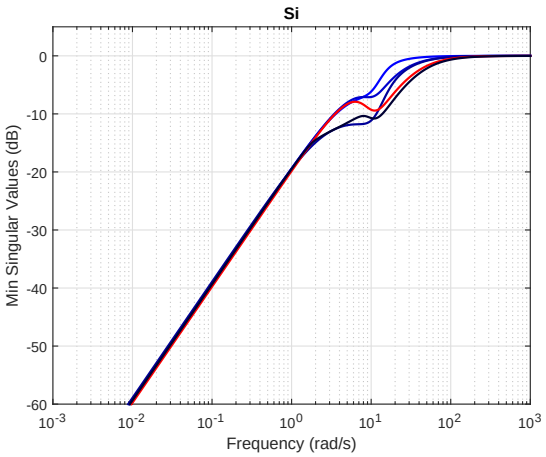

(b) Minimum Singular Value (Model 1)

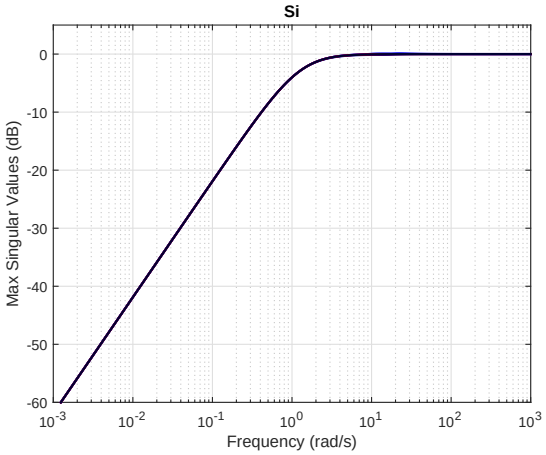

(c) Maximum Singular Value (Model 2)

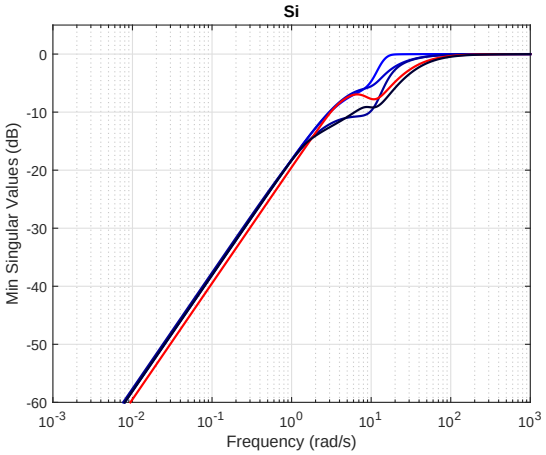

(d) Minimum Singular Value (Model 2)

Figure 5.5: Sensitivity at Input

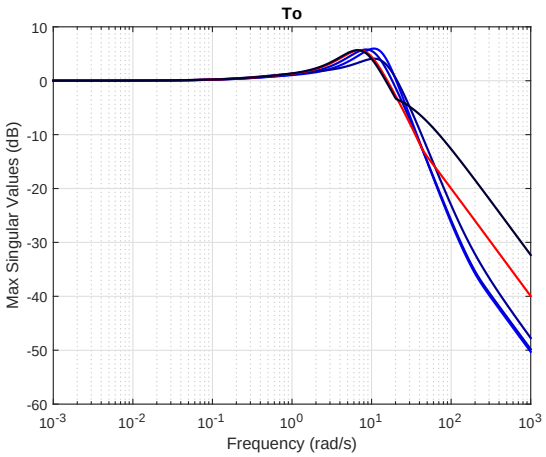

(a) Maximum Singular Value

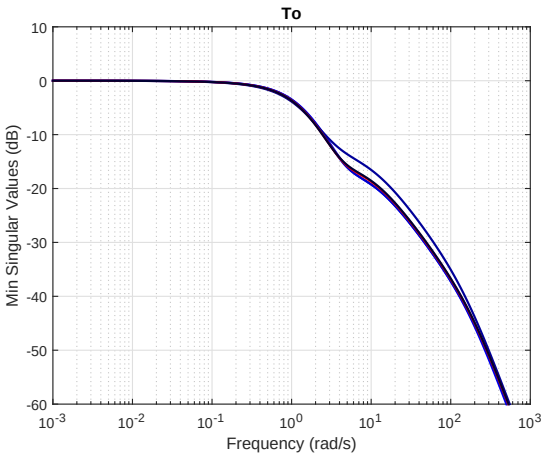

(b) Minimum Singular Value

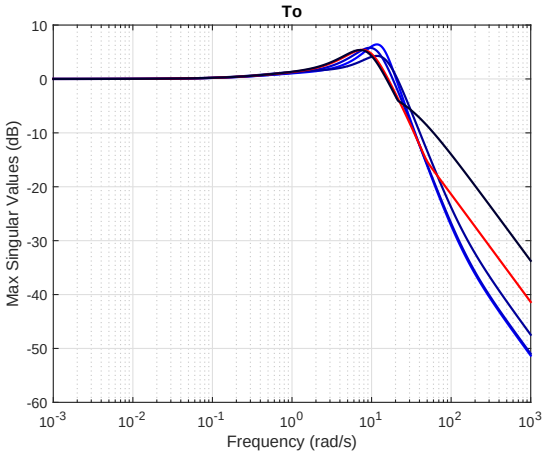

(c) Maximum Singular Value (Model 2)

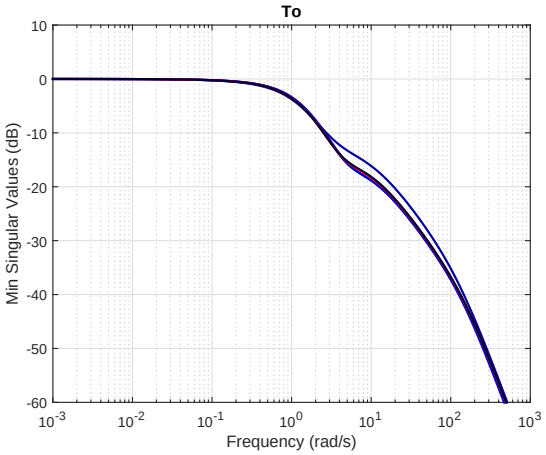

(d) Minimum Singular Value (Model 2)

Figure 5.6: Complementary Sensitivity at Output

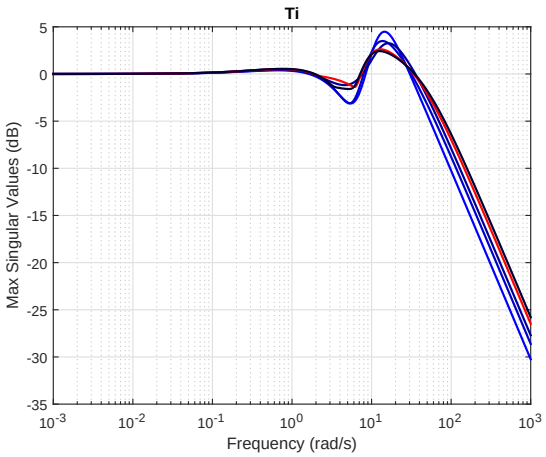

(a) Maximum Singular Value (Model 1)

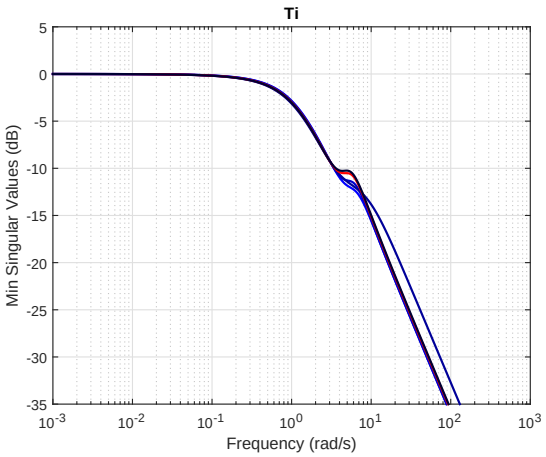

(b) Minimum Singular Value (Model 1)

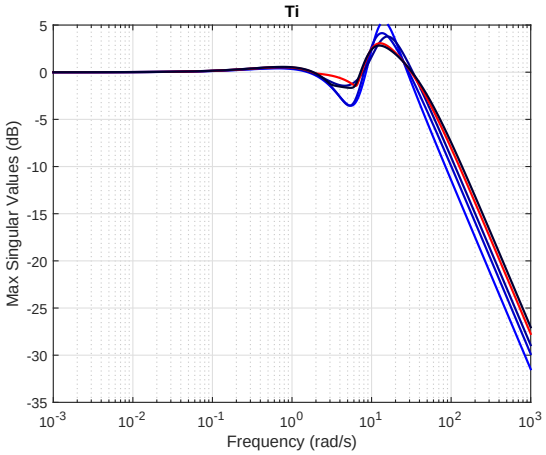

(c) Maximum Singular Value (Model 2)

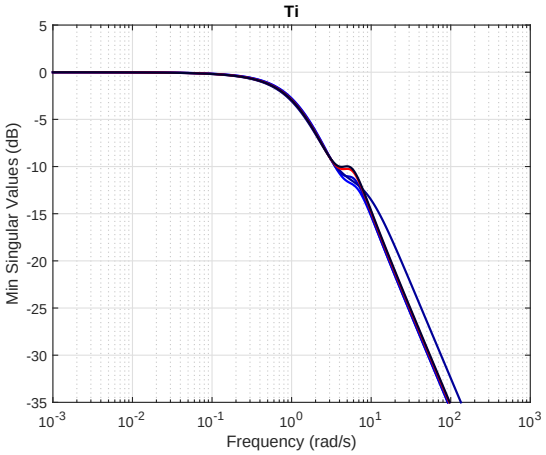

(d) Minimum Singular Value (Model 2)

Figure 5.7: Complementary Sensitivity at Input

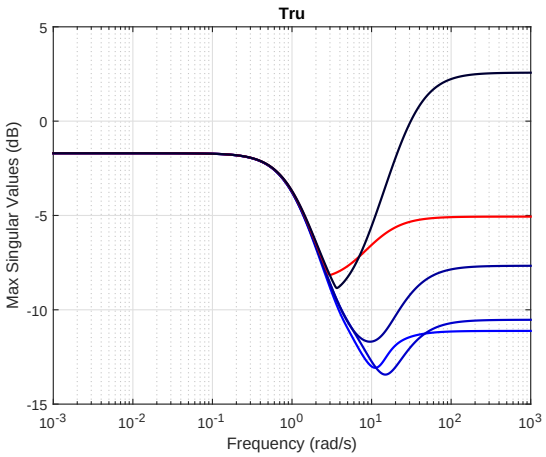

(a) Maximum Singular Value (Model 1)

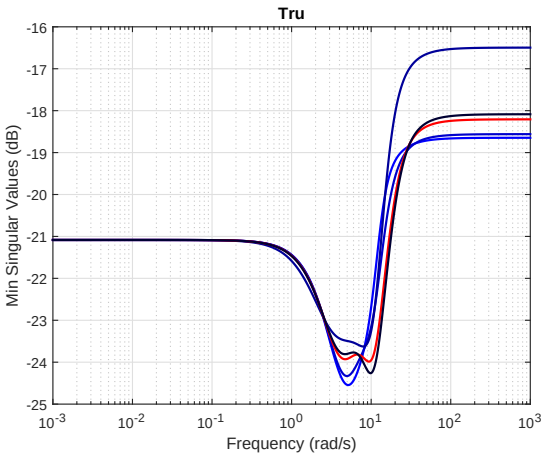

(b) Minimum Singular Value (Model 1)

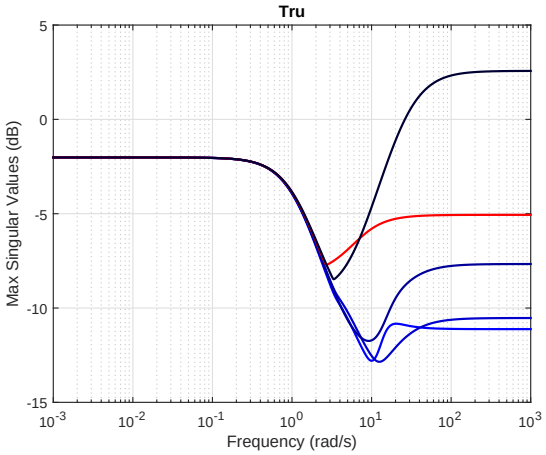

(c) Maximum Singular Value (Model 2)

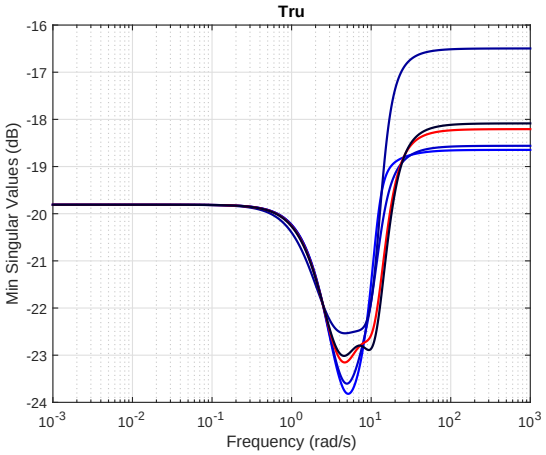

(d) Minimum Singular Value (Model 2)

Figure 5.8: Closed loop Map from Reference to Control

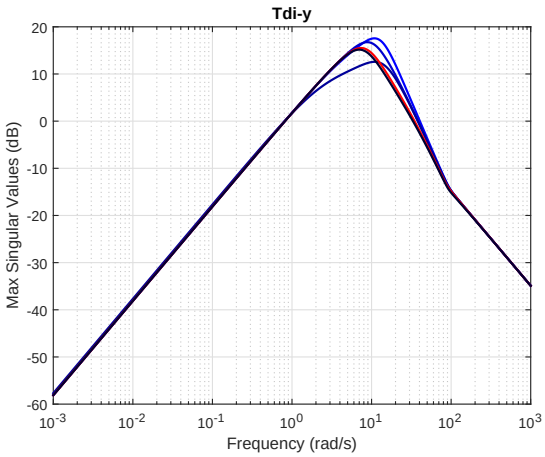

(a) Maximum Singular Value (Model 1)

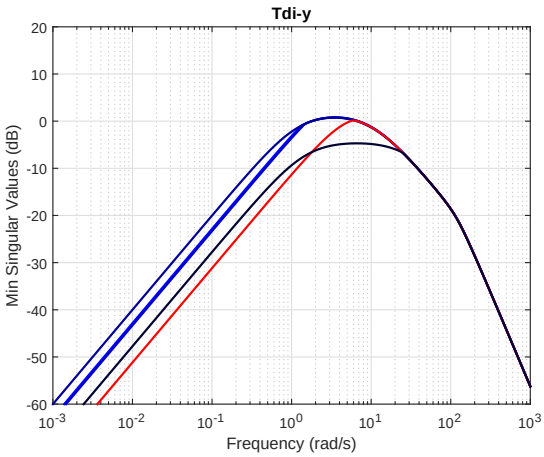

(b) Minimum Singular Value (Model 1)

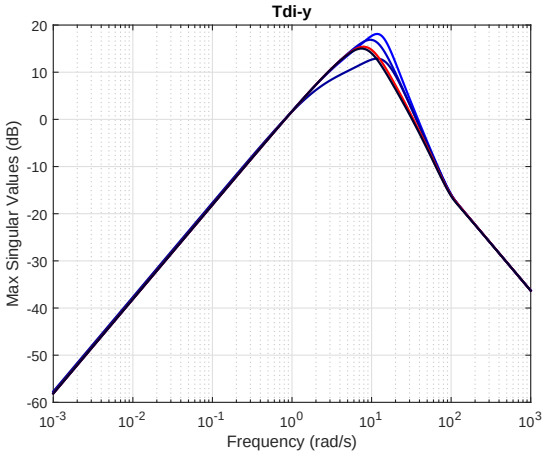

(c) Maximum Singular Value (Model 2)

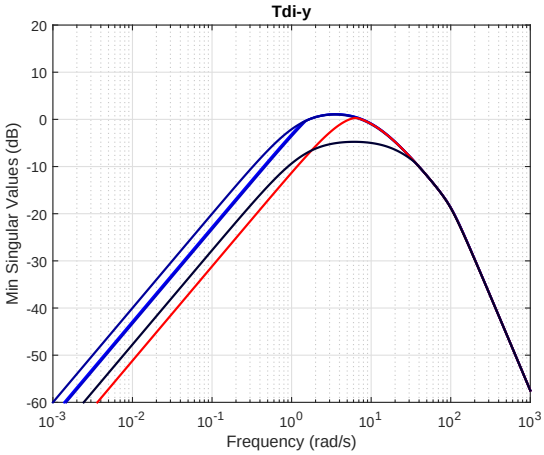

(d) Minimum Singular Value (Model 2)

Figure 5.9: Closed loop Map from Input Disturbance to Plant Output

The design chosen for the step responses shown below, is the one corresponding to L_u crossover frequency ω_c of 48 rad/s. The closed loop eigenvalues are

Table 5.2: Closed loop Eigenvalues

Pole	Damping	ω_n
-35.1	1	35.1
-10.7	1	10.7
-5.16 + j6.64	0.613	8.41
-5.16 - j6.64	0.613	8.41
-1.21	1	1.21
-6.11	1	6.11
-5.48	1	5.48

We now look at the step responses (figures 5.10 - 5.16) of the states and the controls. A step of 0.5 m/s is given to states u and w and the response of linear, averaged nonlinear and nonlinear model is checked. This shows that the hover controller is suitable for small finite forward flight velocities up to 0.5 m/s. We notice in the simulations that beyond 0.6 m/s, the nonlinear system becomes unstable, rendering the hover controller ineffective beyond this speed.

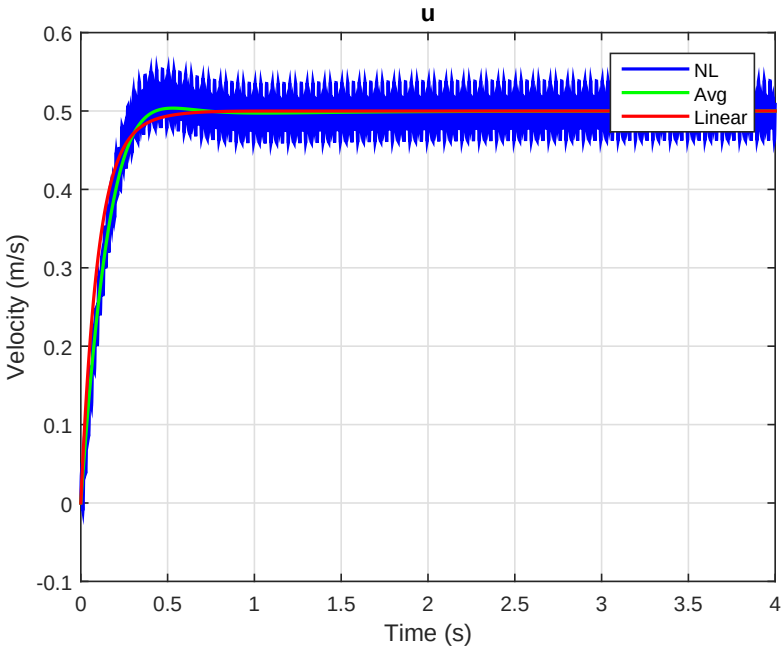

Figure 5.10: Forward Speed (0.5 m/s) Command Following (u)

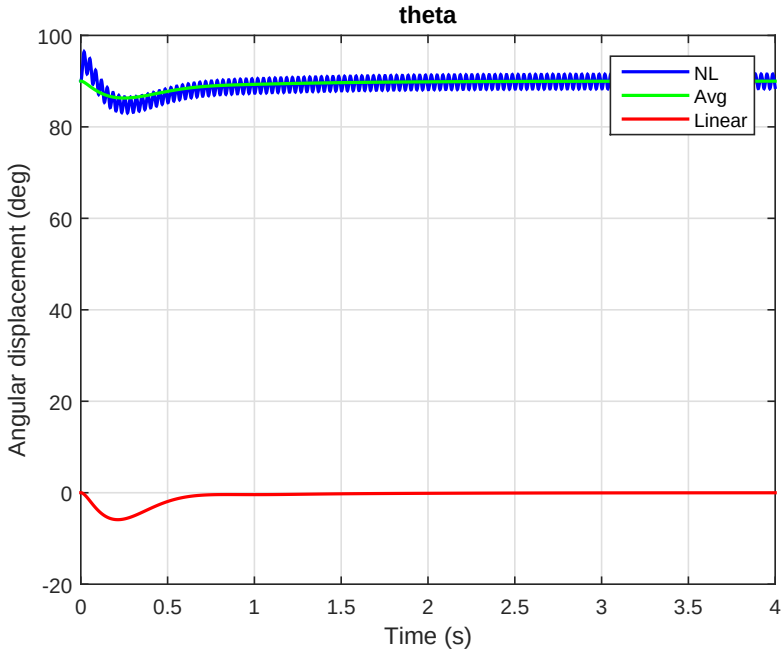

Figure 5.11: Forward Speed Command Following (θ)

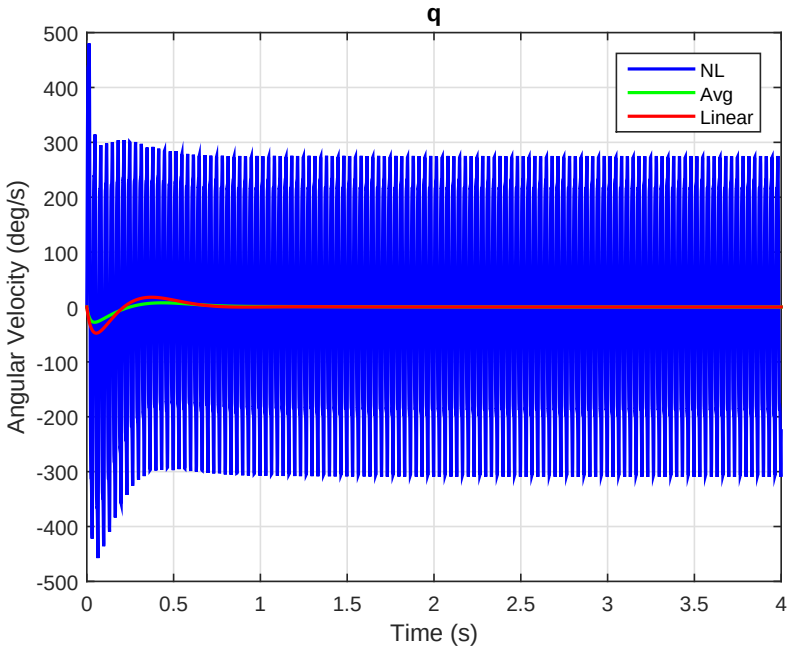

Figure 5.12: Forward Speed Command Following (q)

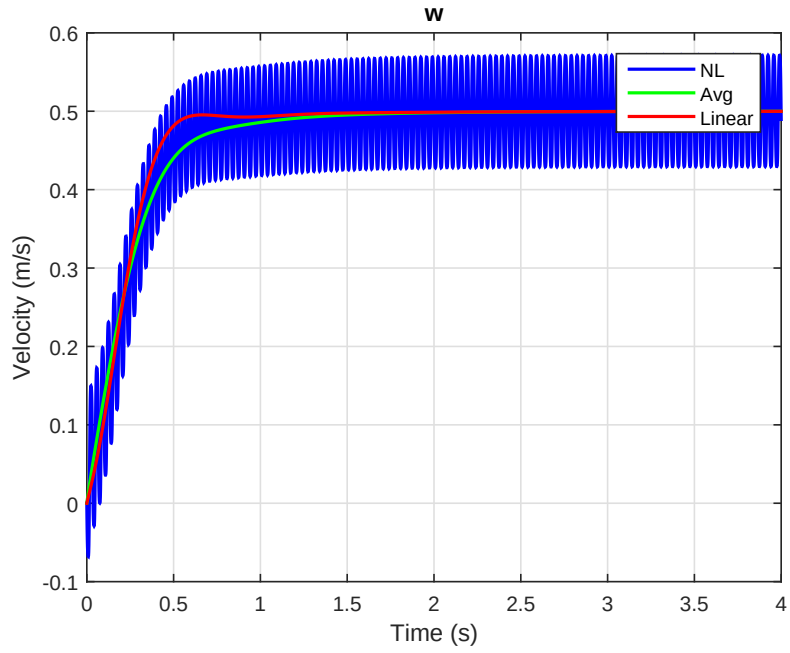

Figure 5.13: Vertical Speed (0.5 m/s) Command Following (w)

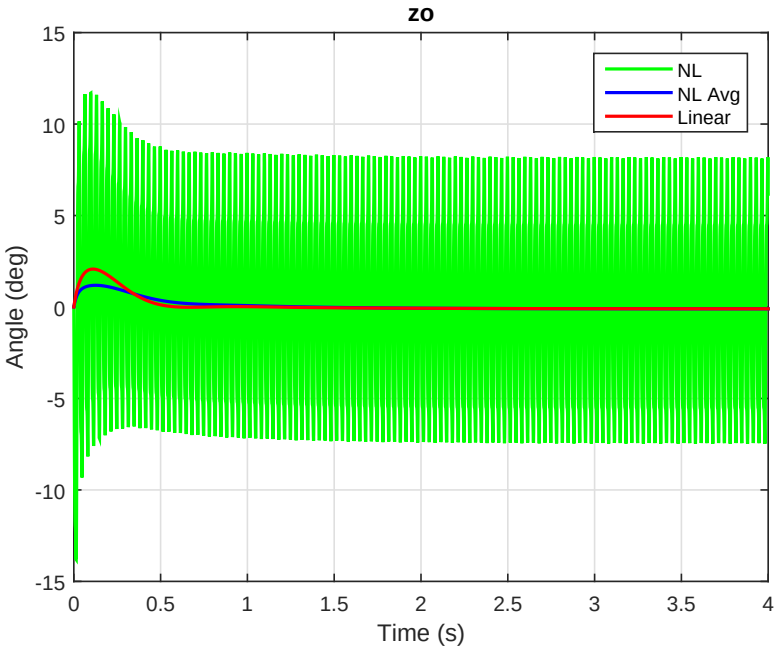

Figure 5.14: Forward Speed Command Following (ϕ_0)

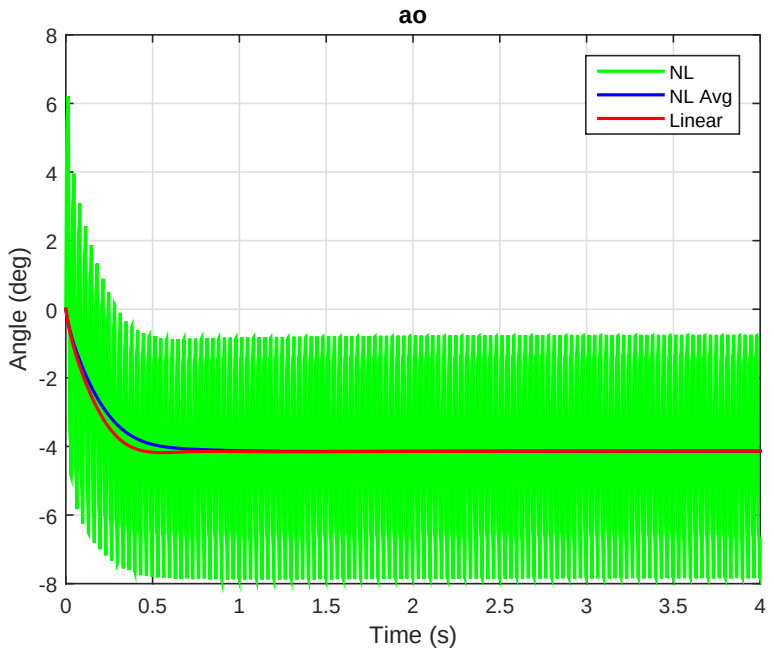

Figure 5.15: Forward Speed Command Following (α_0)

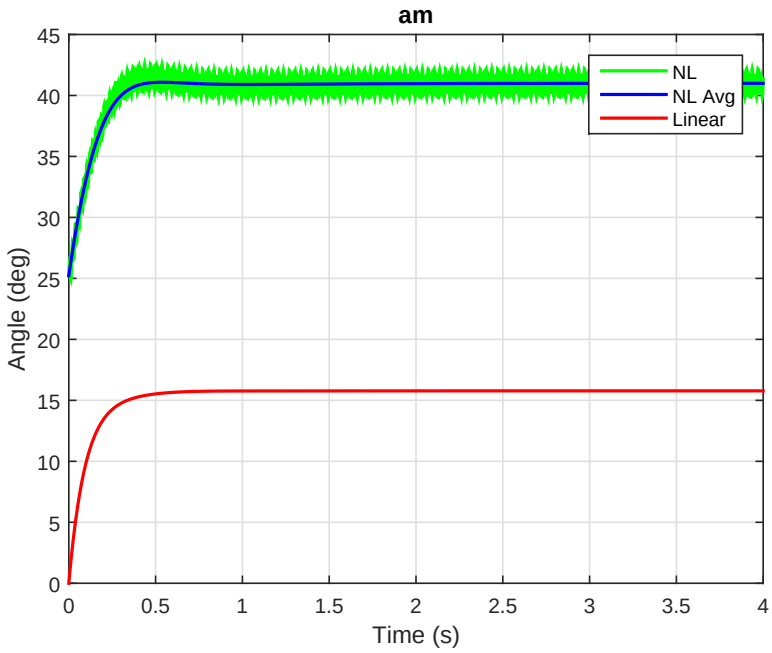

Figure 5.16: Vertical Speed Command Following (α_m)

The resulting closed loop eigenvalues for model 2 are

Table 5.3: Closed loop Eigenvalues

Pole	Damping	ω_n
-29.1	1	29.1
-5.43 + j7.49	0.587	9.25
-5.43 - j7.49	0.587	9.25
-7.2 + j1.85	0.969	7.44
-7.2 - j1.85	0.969	7.44
-1.26	1	1.26
-4.71	1	4.71

The step responses are shown below from figures 5.17 - 5.23. A step of 0.3 m/s is given, showing that the hover controller is valid for a small finite velocities. We noticed in the simulations that beyond 0.4 m/s the hover controller is not able to stabilize the nonlinear system. Responses of all 3 models i.e time varying non-linear, averaged and linear simulations are presented.

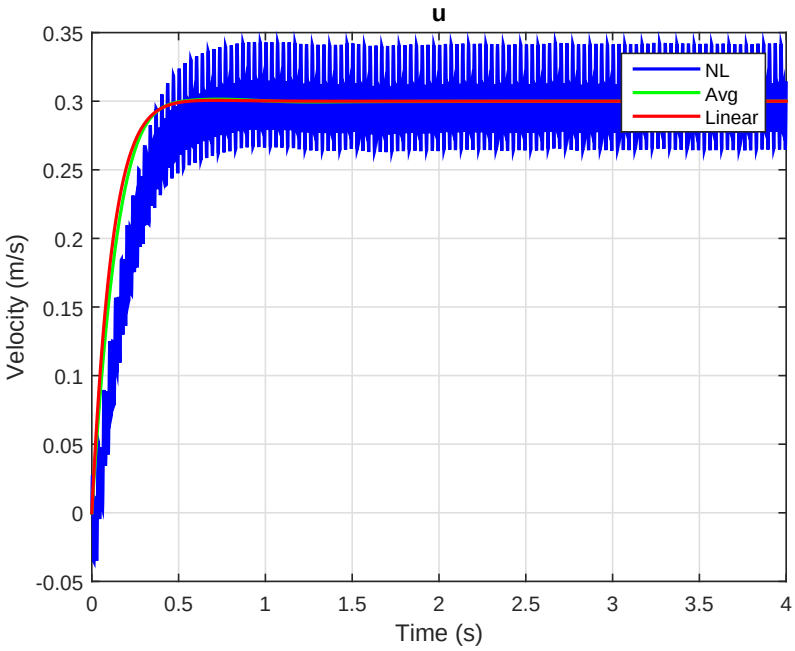

Figure 5.17: Forward Speed (0.3 m/s) Command Following (u)

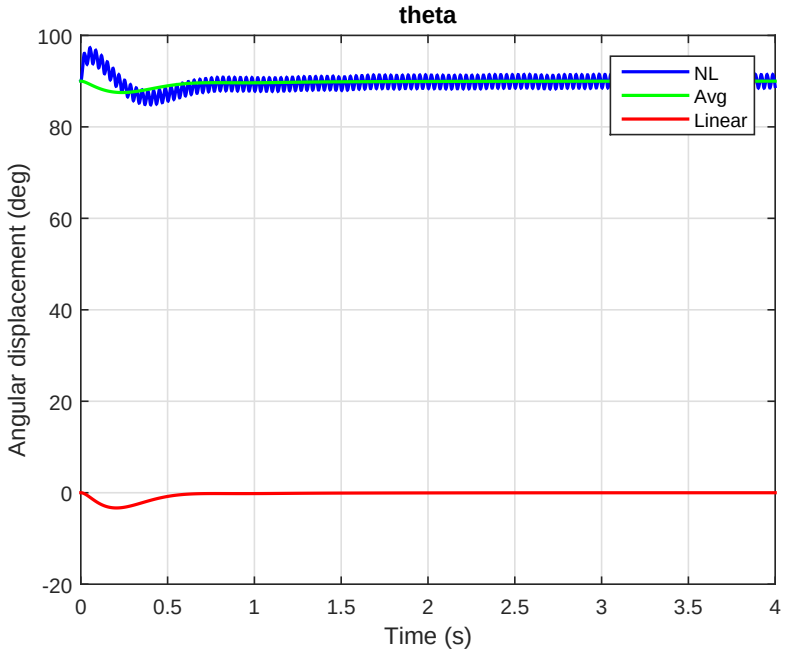

Figure 5.18: Forward Speed Command Following (θ)

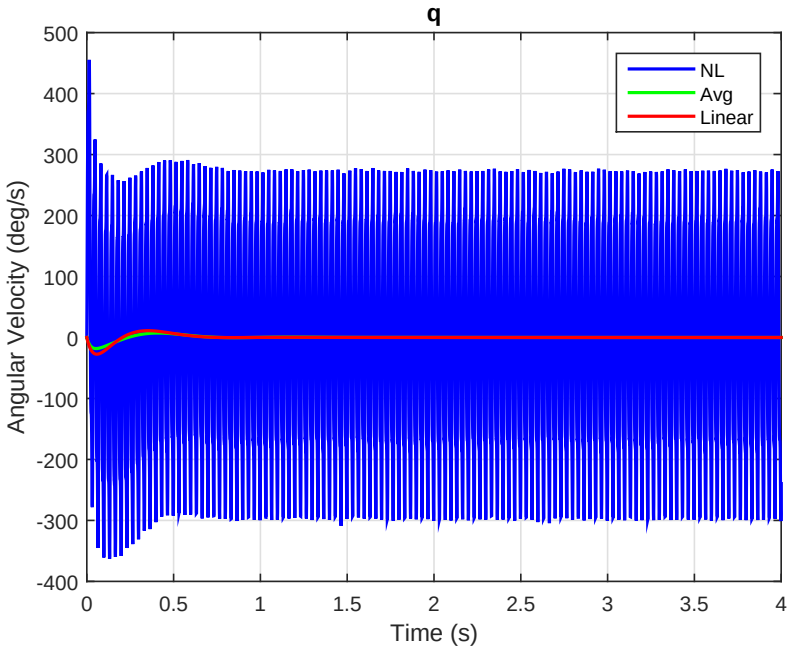

Figure 5.19: Forward Speed Command Following (q)

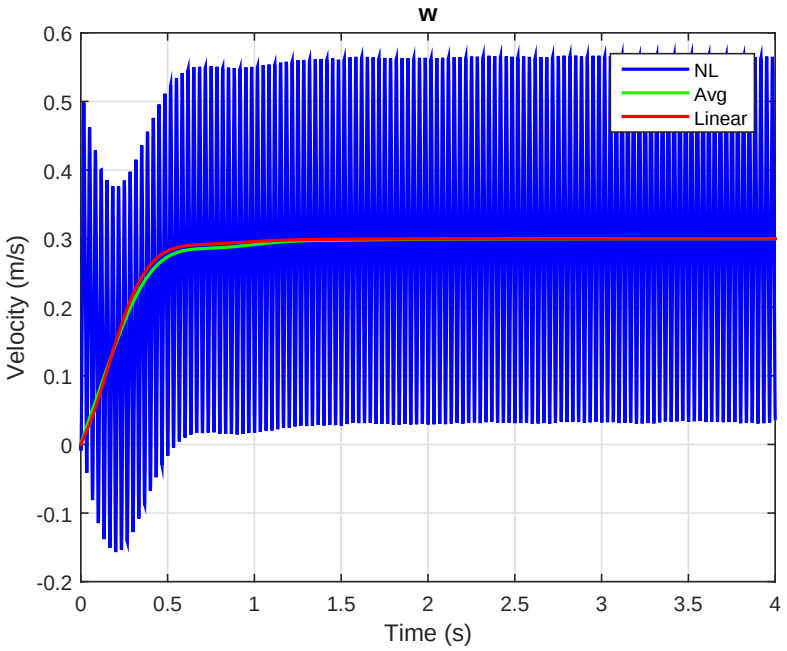

Figure 5.20: Vertical Speed (0.3 m/s) Command Following (w)

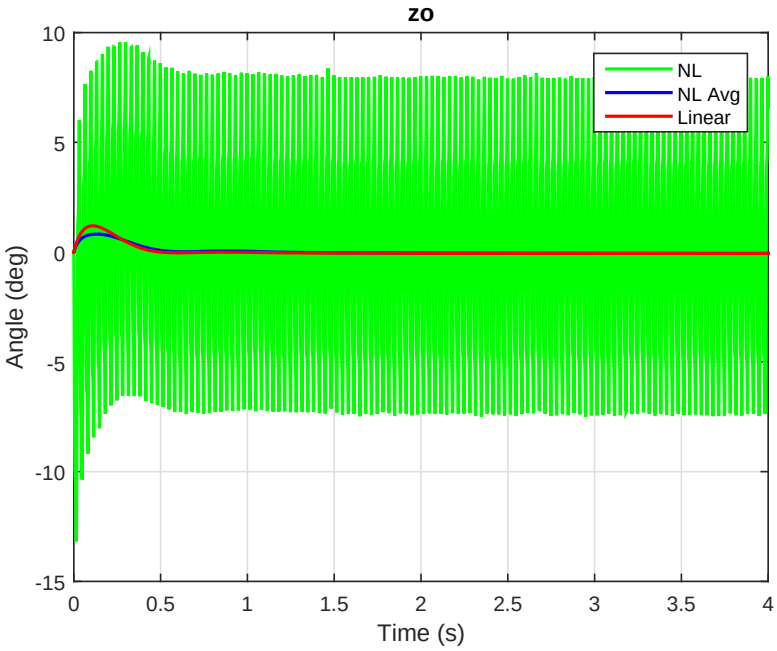

Figure 5.21: Forward Speed Command Following (ϕ_0)

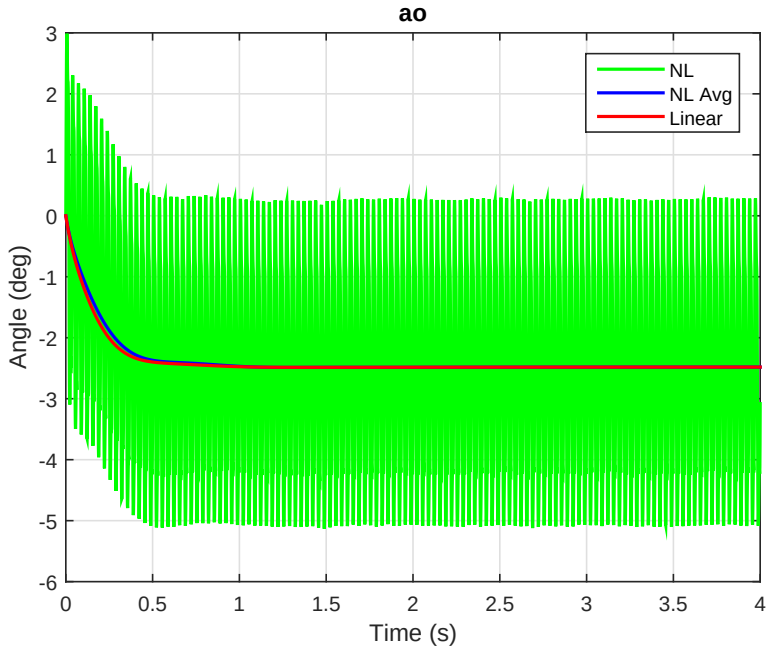

Figure 5.22: Forward Speed Command Following (α_0)

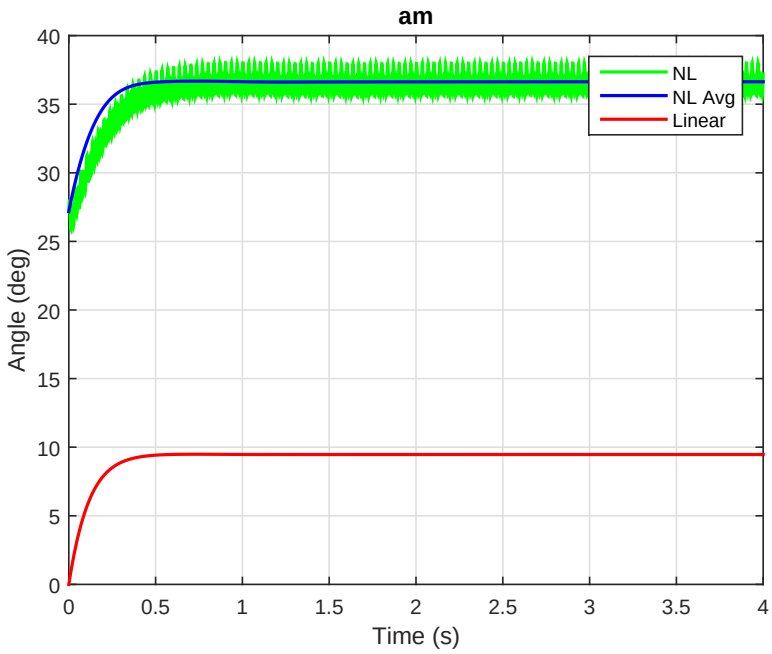

Figure 5.23: Vertical Speed Command Following (α_m)

5.2 Necessity of Wing Inertia Model

The mass of the wings expressed as percentage of body weight is about 6% (considering 2 wings), each wing thus weighs about 3%. This number was increased to around 6% after which the controller failed to stabilize the nonlinear model.

In the figures (5.24 - 5.27) below we see the step responses of the nonlinear model. And even though the controller could tolerate up to 6% of weight, to get satisfactory results, we had to use a controller with higher input bandwidth. We conclude that for the mode considered in this thesis, based on a regular hawkmoth insect, the inertial effect of wings becomes significant and needs to be modeled at around 6%. One can get by ignoring the wing dynamics if closed loop feedback control is employed, unless the wing mass is extremely low $\sim$ 1% (which is what most insects have), in which case one can use model 1 for all practical purposes.

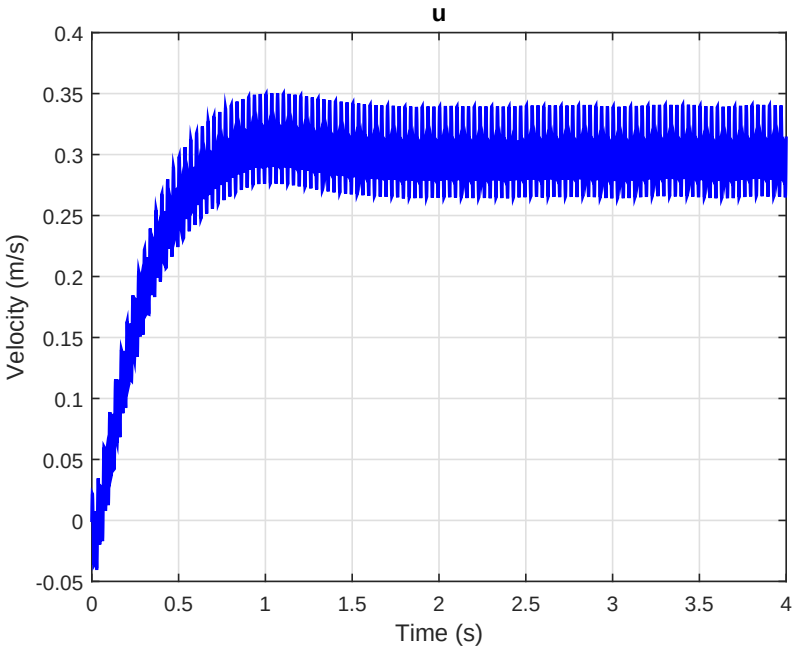

Figure 5.24: 3 Times Higher Wing Weight; Forward Speed Command Following (u)

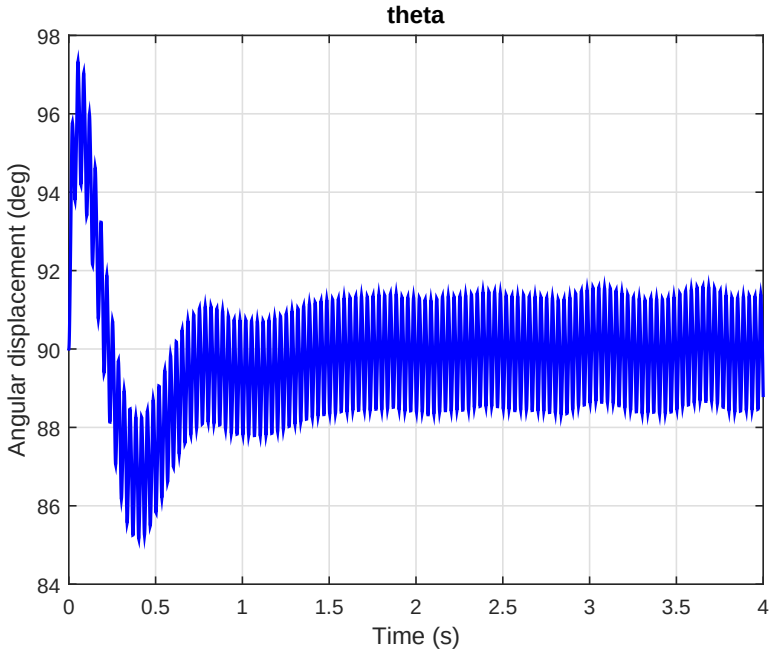

Figure 5.25: 3 Times Higher Wing Weight; Forward Speed Command Following (θ)

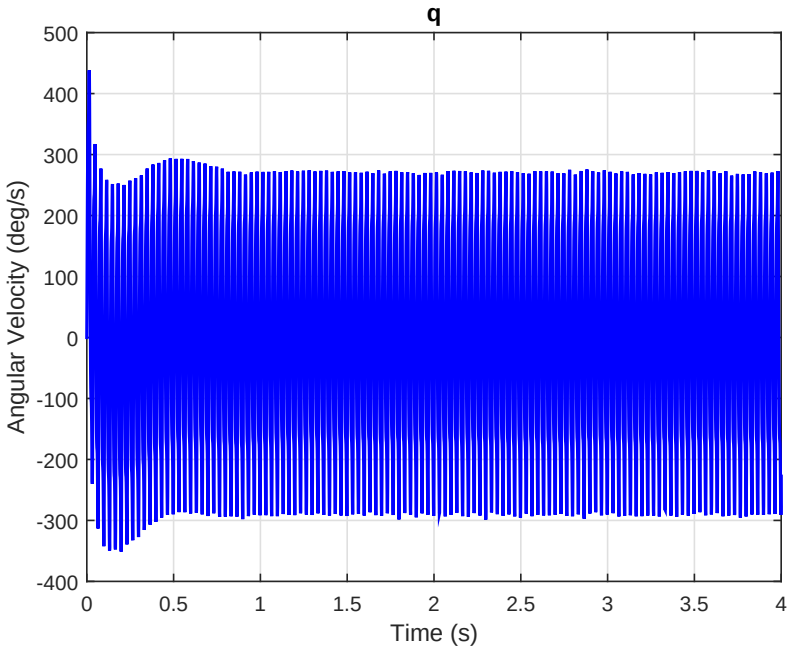

Figure 5.26: 3 Times Higher Wing Weight; Forward Speed Command Following (q)

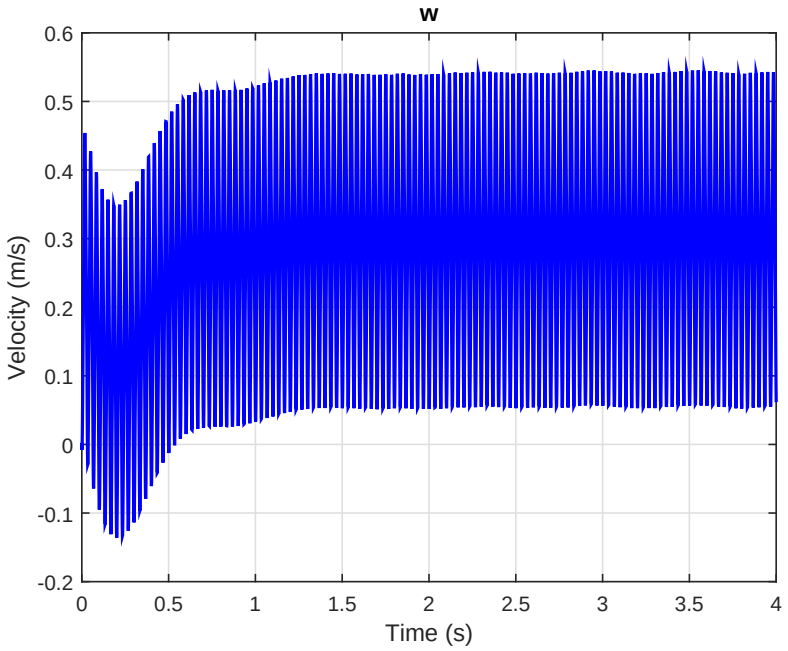

Figure 5.27: 3 Times Higher Wing Weight; Vertical Speed Command Following (w)

5.3 Control for Wing Inertia Model

In this section a controller is designed for model 2 and tested on the first model. Starting with the minimum bandwidth constraint, LQR weighting matrices were optimized. The resulting design was tested on the original model. As expected, it was able to stabilize it. The resulting parameters are shown in the following table.

Table 5.4: closed loop Properties

Model	Min. ζ	Min. T_s	L_u ω_c
II	0.454	3.014	28.4
I	0.568	3.14	32.4

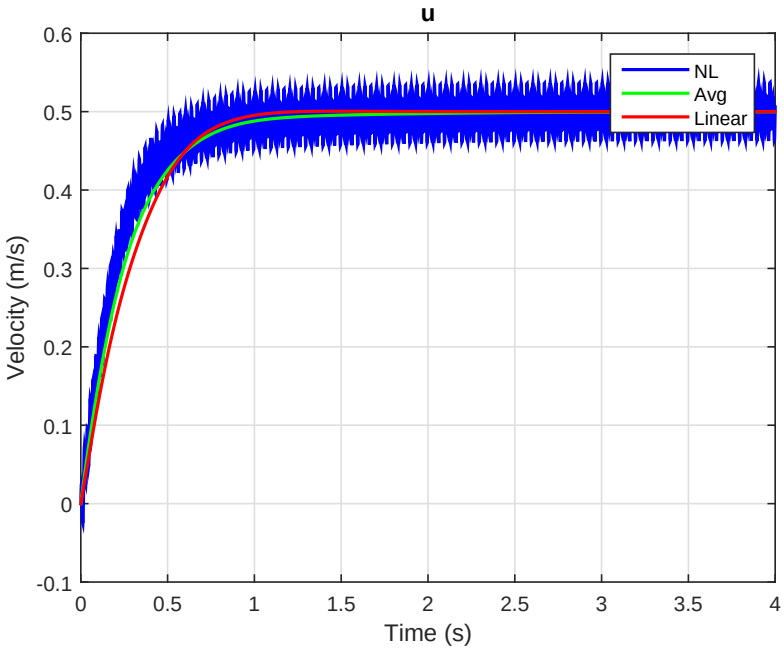

Figure 5.28: Forward Speed (0.1 m/s) Command Following

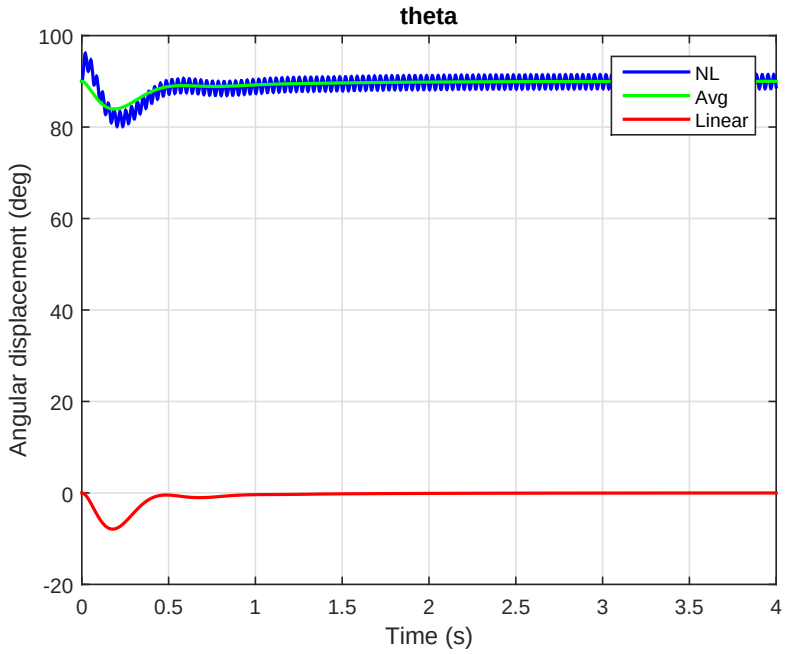

Figure 5.29: Forward Speed Command Following (θ)

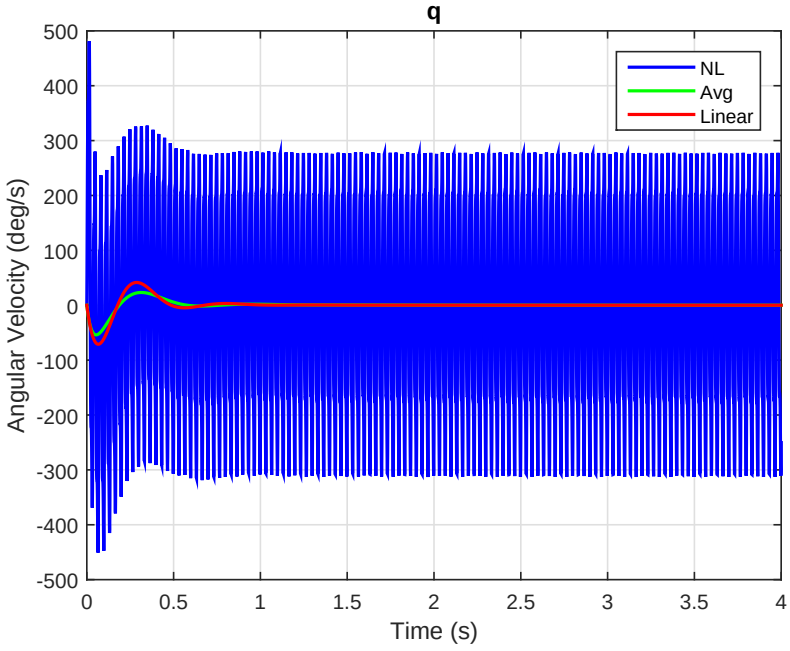

Figure 5.30: Forward Speed Command Following (q)

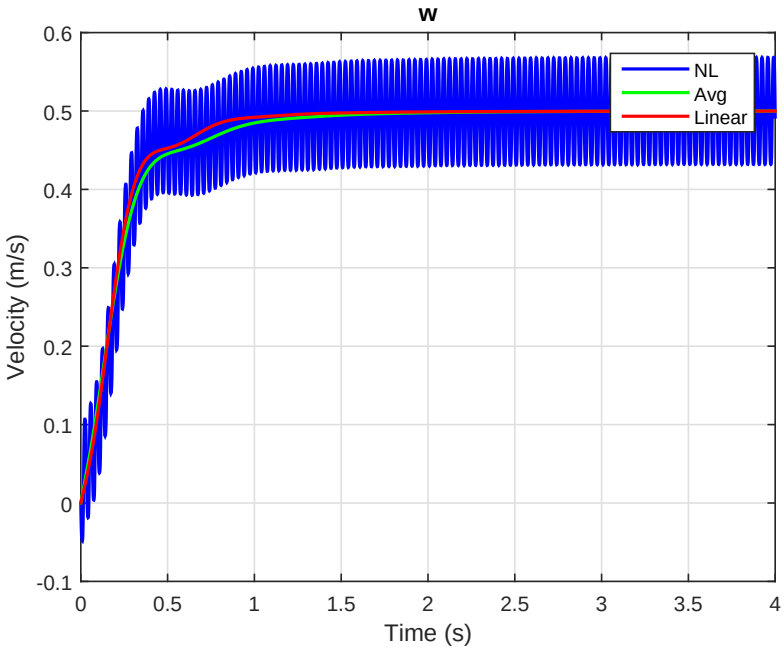

Figure 5.31: Vertical Speed (0.1 m/s) Command Following

5.4 Control of Model 3 - Body and Wing Dynamics

The discussion in this section is still under development. However we would like to present preliminary discussion that highlights the key aspects of the control methodology opted. The model was presented in equation 2.28. But it included pitch angle α dynamics too, in this section however, we are considering a modified version of 2.28, i.e. without α dynamics. Thus the state vector is $\begin{bmatrix} u & w & \theta & q & \phi & \dot{\phi} \end{bmatrix}^T$. In the previous models the flapping angle of the wing i.e. $\phi(t) = \phi_0 - \phi_m \sin(\omega t)$ was imposed on the body. However in this model, the flapping angle becomes a state and it is an outcome of the wing dynamics. The last 2 equations of 2.28 show that the wing dynamics includes its own inertia and terms representing the coupling between body and wing. Given an input torque to the wings, these equations need to be solved, for the wing degree of freedom/state (ϕ).

A Hierarchical controller structure like the one shown in figure 5.32 is being used.

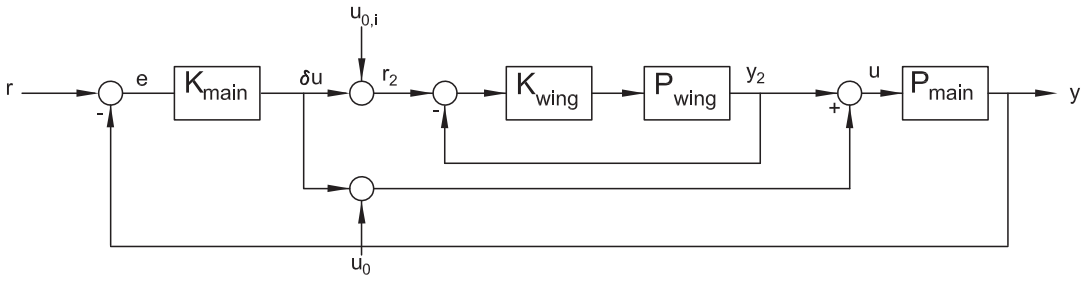

Figure 5.32: Hierarchical Control Structure for Model 3

Two loops, outer and inner are being used. Inner loop stabilizes the wing attitude while the outer loop stabilizes the body attitude. The outer loop controller is the same LQR that was designed in the previous sections. The reference to the outer loop remain the same i.e. the reference velocities and pitch angle $\begin{bmatrix} u & w & \theta \end{bmatrix}^T$. The outer controller's output corresponding to flapping state offset (ϕ_0) channel is added to the desired sinusoid signal ($\phi_m \sin(wt)$) and fed into the controller for the inner loop. Inner loop is SISO and state feedback LQR can be used to control this loop. The controller for the inner loop is however augmented with $\frac{1}{s^2+\omega^2}$, to track the sinusoid reference signal.

The flapping wing is modeled as

$$\tau = Js^2 + Bs + K \tag{5.2}$$

The damping and spring constant of the wing hinge have been chosen to mimic available actuator parameters. Although the coupling does not show up in the linear model, the controller will be designed such that is it robust to the body coupling terms. The controller design is still in progress. And the simulations will be presented in a technical paper that will be released soon.

5.5 Summary

In this chapter it was seen that although hover is not an equilibrium point for the original time varying system, it can be stabilized about a periodic trajectory, average of which, is an equilibrium point for the averaged system. Averaging is an approximation and the closeness of this approximation and original system depends on the ϵ term introduced in chapter 3. The role of ϵ is played by frequency which is 188 rad/s roughly. Thus averaging works in the case of such systems where the ϵ is small. As seen from the simulations, first order averaging works quite well in this case. Second order averaging as seen in chapter 3 didn't yield significant change in the linearization. Also note the approximation holds true for a time scale $1/\epsilon$. On this small time scale, the response is mostly determined by its average.

We will now answer precisely some of the questions that were posed in the beginning of this chapter. The closed loop bandwidth that should be sufficiently small, for averaging to be valid, is T_o. T_o is the closed loop map from reference to output. It was observed that more than 30 rad/s crossover frequency which is roughly 1/6th of the forcing frequency, the nonlinear system is not able to stabilize.

The wingless model is sufficient for low wing mass, satisfactory results are obtained for each wing mass up to 6% of body weight. An interesting point to note here, is that the averaged model stabilizes and follows quite well with the linear model. The necessity of modeling the wing inertial effect and designing a controller for this model becomes essential with a wing mass of about 6% of body weight for the case considered here.

The hover controller is also able to stabilize the model up to small forward velocities. For model 1, up to 0.6 m/s in both directions (x_b, z_b) of the body, the controller worked well. Beyond this speed, a cruise controller would have to be designed. This

upper limit of the forward speed decreased when the controller was operated on model 2.

Lastly a controller designed for the wing inertial model is also able to stabilize the wingless model with satisfactory responses.

Chapter 6

CONCLUSION AND FUTURE RESEARCH

In this thesis, modeling and control of flapping flight for robotic insects were analyzed in detail. The most important contribution of this thesis is to show how modeling can be dealt in different ways, how and when it can be simplified, what underlying assumptions are being made in this simplification process and when is it safe or unsafe to make these. Second important point of discussion was averaging; how it applies to the MAV system, and whether higher order approximations are necessary. We now conclude the the research presented.

6.1 Conclusion

Insect sized micro aerial vehicles that can especially ape their flight capabilities would truly revolutionize surveillance. However due to their flapping flight and thus added degrees of freedom of the wings, modeling is a challenge. Owing to the flapping nature of the wing (actuator), the force field is basically a high frequency periodic vector field. Analyzing the effect of this fast changing system on the slow system entails knowledge of averaging/Floquet theory. Achieving stability via vibrations makes the system more complicated. Even more challenging is the hardware to build such robots at an insect level. However few researchers have been successful in building flapping vehicles. The area is thus still fresh and much research needs to be done along these directions. In this thesis, we have identified two partially answered areas of research, namely modeling of the wings and validity of averaging theory. we have sincerely tried addressing these problematic areas through controls perspective.
In chapter 2 all three models were derived from the basic principles. Many researchers

have opted for the simplest model that is the wingless body. The reasoning behind this, is that the wings mass simply doesn't matter. Each wing roughly is a meager 1% of the body weight. As analyzed in chapter 5 this model is sufficient for good 6% figure. This model owing to its simplicity is very amenable from a real time computation perspective. However its validity comes under question when the wing mass increases. The figure of 6% was true in this case, however a similar analysis needs to be done if the wing mass exceeds 3% and/or the flapping frequency is low, which contributes significantly to the inertial effect of the wing.

The third model is what the actual implemented system would look like. In reality the wing's state will be driven by a motor with its own dynamics. In the second model, the flapping degree of freedom was imposed. As long as the modes (poles) of the wing system are far away from the body's modes, the two models will look very similar. Again the poles being far from the body's poles directly means that the mass of the wings is very small.

Having analyzed all 3 models, we comment on the need of higher order averaging. As seen and discussed in the third chapter, the use of such perturbation method is only possible if the ϵ is strictly small and positive. If this is not the case, the validity of using averaging theory falls through. Having said that, however higher order averaging is useful in improving the accuracy on the order of (ϵ^k) and in determining the stability of systems that have poles on the imaginary axis from first order averaging. However since the eigenvalues were relatively far away from the imaginary axis, the stability of the linear map didn't change much. In any case the change in eigenvalue shift would be on the order of (ϵ^2). Hence we concluded that using feedback control, first order averaging is sufficient.

6.2 Future Direction

Flapping wing robots that can truly ape insects is far from reality, till then the possibilities are many.

Advanced Models: Hover was the main flight condition in this thesis. And the aerodynamic model considered was a very simple model. The major limitations of this model are, ignoring aero-elastic effects and modeling the wings as rigid. Though the dynamic model could be easily extended to forward flight or lateral motion, the aerodynamics and the relative significance of flight controls would change considerably. Most of the aerodynamic models found in literature concentrate on hover, the current model would render ineffective. Secondly the wing motion was parameterized such that the hover was achieved easily, however insect use many more kinematic parameters other then the ones used here in forward flight, this map of controls to degrees of freedom of wings as a function of flight condition after having incorporated the right aerodynamics would have to be studied.

Trajectory Planning: Insects are able to perform sharp saccades of 90 °. To be able to mimic the fast maneuvers of insects, the control system needs to be made faster i.e. higher bandwidth. Not much literature can be found on path planning of such maneuvers. Optimal trajectory planning to achieve a certain goal is definitely challenging especially with limited controls and bandwidth.

Actuator and Sensory System: The actuator and sensory dynamics were ignored in this thesis, but in reality incorporating these could change the structure of system. In reality all actuators have saturation limits and and they have their own dynamics. Capturing these dynamics is crucial for design. Sensors too have their limitations. They have to process information fast and translate the information into

commands for the system for stabilization and navigation.They have their own dynamics. All these practical, real life situations would have to be included in the design because reality will be even worse.

Energy Efficiency Consideration : The wing kinematics were adopted based on flight condition, however for optimality energy should be the criterion. The objective is to perform the desired flight with minimum energy consuming kinematics. The trade off between performance and efficiency is always a good question to ask. However, not much research has looked from power perspective. A study of the trade offs between maneuvers and power requirement can help in the design of better vehicles.

Modeling Uncertainty and Robust Control: Uncertainty modeling and analysis done here can be done in a much more guaranteed, control theoretic framework under mu analysis. Mu guarantees performance and stability properties of the linear plant with respect to uncertainties. It gives bounds on how much uncertainty the plant can tolerate. This would make the analysis of the wing model proper and rigorous.

Test Bench: Simulations only tell half the truth, the results found should be tested experimentally on a test bench. Ultimately building these micro or nano aerial vehicles will be extremely challenging because of the size limitation. Without sacrificing on the performance too much, maintaining the insect level size will be difficult. New manufacturing schemes have to be looked into to go to a true micro scale.

REFERENCES

Alexander, D. E., *Nature's flyers: birds, insects, and the biomechanics of flight* (JHU Press, 2004).

Ansari, S., R. Żbikowski and K. Knowles, "Aerodynamic modelling of insect-like flapping flight for micro air vehicles", Progress in Aerospace Sciences **42**, 2, 129–172 (2006a).

Ansari, S., R. Żbikowski and K. Knowles, "Non-linear unsteady aerodynamic model for insect-like flapping wings in the hover. part 1: methodology and analysis", Proceedings of the Institution of Mechanical Engineers, Part G: Journal of Aerospace Engineering **220**, 2, 61–83 (2006b).

Ansari, S., R. Żbikowski and K. Knowles, "Non-linear unsteady aerodynamic model for insect-like flapping wings in the hover. part 2: implementation and validation", Proceedings of the Institution of Mechanical Engineers, Part G: Journal of Aerospace Engineering **220**, 3, 169–186 (2006c).

Berman, G. J. and Z. Wang, "Energy-minimizing kinematics in hovering insect flight", Journal of Fluid Mechanics **582**, 153–168 (2007).

Bolender, M. A., "Rigid multi-body equations-of-motion for flapping wing mavs using kanes equations", in "AIAA Guidance, Navigation, and Control Conference, AIAA Paper", vol. 6158 (2009).

Deng, X., L. Schenato and S. S. Sastry, "Flapping flight for biomimetic robotic insects: Part ii-flight control design", Robotics, IEEE Transactions on **22**, 4, 789–803 (2006a).

Deng, X., L. Schenato, W. C. Wu and S. S. Sastry, "Flapping flight for biomimetic robotic insects: Part i-system modeling", Robotics, IEEE Transactions on **22**, 4, 776–788 (2006b).

Dickinson, M. H., F.-O. Lehmann and S. P. Sane, "Wing rotation and the aerodynamic basis of insect flight", Science **284**, 5422, 1954–1960 (1999).

Dickson, W. B. and M. H. Dickinson, "The effect of advance ratio on the aerodynamics of revolving wings", Journal of Experimental Biology **207**, 24, 4269–4281 (2004).

Dickson, W. B., A. D. Straw and M. H. Dickinson, "Integrative model of drosophila flight", AIAA journal **46**, 9, 2150–2164 (2008).

Dietl, J. M. and E. Garcia, "Stability in hovering ornithopter flight", in "The 15th International Symposium on: Smart Structures and Materials & Nondestructive Evaluation and Health Monitoring", pp. 69300N–69300N (International Society for Optics and Photonics, 2008).

Dudley, R., *The biomechanics of insect flight: form, function, evolution* (Princeton University Press, 2002).

Dudley, R. and C. Ellington, "Mechanics of forward flight in bumblebees: I. kinematics and morphology", Journal of Experimental Biology **148**, 1, 19–52 (1990a).

Dudley, R. and C. Ellington, "Mechanics of forward flight in bumblebees: Ii. quasi-steady lift and power requirements", Journal of Experimental Biology **148**, 1, 53–88 (1990b).

Ellington, C., "The aerodynamics of hovering insect flight. ii. morphological parameters", Philosophical Transactions of the Royal Society of London. Series B, Biological Sciences pp. 17–40 (1984a).

Ellington, C., "The aerodynamics of hovering insect flight. iii. kinematics", Philosophical Transactions of the Royal Society of London. Series B, Biological Sciences pp. 41–78 (1984b).

Ellington, C., "The aerodynamics of hovering insect flight. iv. aeorodynamic mechanisms", Philosophical Transactions of the Royal Society B: Biological Sciences **305**, 1122, 79–113 (1984c).

Ellington, C. P., "The novel aerodynamics of insect flight: applications to micro-air vehicles", Journal of Experimental Biology **202**, 23, 3439–3448 (1999).

Ellington, C. P., C. Van Den Berg, A. P. Willmott and A. L. Thomas, "Leading-edge vortices in insect flight", (1996).

Epstein, M., S. Waydo, S. B. Fuller, W. Dickson, A. Straw, M. H. Dickinson and R. M. Murray, "Biologically inspired feedback design for drosophila flight", in "American Control Conference, 2007. ACC'07", pp. 3395–3401 (IEEE, 2007).

Faruque, I. and J. Sean Humbert, "Dipteran insect flight dynamics. part 1 longitudinal motion about hover", Journal of Theoretical Biology **264**, 2, 538–552 (2010).

Greenwood, D. T., *Principles of dynamics* (Prentice-Hall Englewood Cliffs, NJ, 1988).

Hedrick, T. and T. Daniel, "Flight control in the hawkmoth manduca sexta: the inverse problem of hovering", The journal of experimental Biology **209**, 16, 3114–3130 (2006).

Humbert, J. S. and I. A. Faruque, "Analysis of insect-inspired wingstroke kinematic perturbations for longitudinal control", Journal of Guidance, Control, and Dynamics **34**, 2, 618–623 (2011).

Karásek, M. and A. Preumont, "Simulation of flight control of a hummingbird like robot near hover", Engineering Mechanics p. 322 (2012).

Khan, Z. A. and S. K. Agrawal, "Modeling and simulation of flapping wing micro air vehicles", in "ASME 2005 International Design Engineering Technical Conferences and Computers and Information in Engineering Conference", pp. 871–879 (American Society of Mechanical Engineers, 2005).

Khan, Z. A. and S. K. Agrawal, "Control of longitudinal flight dynamics of a flapping-wing micro air vehicle using time-averaged model and differential flatness based controller", in "American Control Conference", vol. 9, pp. 5284–5289 (2007).

Murdock, J. A., *Perturbations: theory and methods*, vol. 27 (Siam, 1999).

Oppenheimer, M. W., D. B. Doman and D. O. Sigthorsson, "Dynamics and control of a biomimetic vehicle using biased wingbeat forcing functions", Journal of guidance, control, and dynamics **34**, 1, 204–217 (2011).

Orlowski, C. T. and A. R. Girard, "Averaging of the nonlinear dynamics of flapping wing micro air vehicles for symmetrical flapping", AIAA Paper **1228** (2011a).

Orlowski, C. T. and A. R. Girard, "Modeling and simulation of nonlinear dynamics of flapping wing micro air vehicles", AIAA journal **49**, 5, 969–981 (2011b).

Orlowski, C. T. and A. R. Girard, "Dynamics, stability, and control analyses of flapping wing micro-air vehicles", Progress in Aerospace Sciences **51**, 18–30 (2012).

Phan, H. V., Q. V. Nguyen, Q. T. Truong, T. Van Truong, H. C. Park, N. S. Goo, D. Byun and M. J. Kim, "Stable vertical takeoff of an insect-mimicking flapping-wing system without guide implementing inherent pitching stability", Journal of Bionic Engineering **9**, 4, 391–401 (2012).

Ramamurti, R. and W. C. Sandberg, "A three-dimensional computational study of the aerodynamic mechanisms of insect flight", Journal of Experimental Biology **205**, 10, 1507–1518 (2002).

Ristroph, L., G. Ristroph, S. Morozova, A. J. Bergou, S. Chang, J. Guckenheimer, Z. J. Wang and I. Cohen, "Active and passive stabilization of body pitch in insect flight", Journal of The Royal Society Interface **10**, 85, 20130237 (2013).

Sanders, J. A., F. Verhulst and J. Murdock, *Averaging methods in nonlinear dynamical systems*, vol. 59 (Springer, 2007).

Sane, S. P., "The aerodynamics of insect flight", The journal of experimental Biology **206**, 23, 4191–4208 (2003).

Sane, S. P. and M. H. Dickinson, "The control of flight force by a flapping wing: lift and drag production", Journal of experimental biology **204**, 15, 2607–2626 (2001).

Sane, S. P. and M. H. Dickinson, "The aerodynamic effects of wing rotation and a revised quasi-steady model of flapping flight", Journal of Experimental Biology **205**, 8, 1087–1096 (2002).

Serrani, A., B. E. Keller, M. A. Bolender and D. B. Doman, "Robust control of a 3-dof flapping wing micro air vehicle", in "Proceedings of the AIAA guidance, navigation, and control conference. Toronto, Ontario, Canada: AIAA", pp. 2–5 (2010).

Sun, M., "Insect flight dynamics: stability and control", Reviews of Modern Physics **86**, 2, 615 (2014).

Sun, M., J. Wang and Y. Xiong, "Dynamic flight stability of hovering insects", Acta Mechanica Sinica **23**, 3, 231–246 (2007).

Taha, H. E., *Mechanics of Flapping Flight: Analytical Formulations of Unsteady Aerodynamics, Kinematic Optimization, Flight Dynamics, and Control*, Ph.D. thesis, Virginia Polytechnic Institute and State University (2013).

Taha, H. E., M. R. Hajj and A. H. Nayfeh, "Flight dynamics and control of flapping-wing mavs: a review", Nonlinear Dynamics **70**, 2, 907–939 (2012).

Taylor, G. and A. Thomas, "Animal flight dynamics ii. longitudinal stability in flapping flight", Journal of Theoretical Biology **214**, 3, 351–370 (2002).

Taylor, G. K., "Mechanics and aerodynamics of insect flight control", Biological Reviews **76**, 4, 449–471 (2001).

Vela, P. A., K. A. Morgansen and J. W. Burdick, "Second order averaging methods for oscillatory control of underactuated mechanical systems", in "American Control Conference, 2002. Proceedings of the 2002", vol. 6, pp. 4672–4677 (IEEE, 2002).

Wang, Z. J., "Dissecting insect flight", Annu. Rev. Fluid Mech. **37**, 183–210 (2005).

Willmott, A. P. and C. P. Ellington, "The mechanics of flight in the hawkmoth manduca sexta. i. kinematics of hovering and forward flight.", The Journal of Experimental Biology **200**, 21, 2705–2722 (1997a).

Willmott, A. P. and C. P. Ellington, "The mechanics of flight in the hawkmoth manduca sexta. ii. aerodynamic consequences of kinematic and morphological variation.", The Journal of experimental biology **200**, 21, 2723–2745 (1997b).

Wu, J. and M. Sun, "Control for going from hovering to small speed flight of a model insect", Acta Mechanica Sinica **25**, 3, 295–302 (2009).

Wu, J. H., Y. L. Zhang and M. Sun, "Hovering of model insects: simulation by coupling equations of motion with navier–stokes equations", Journal of Experimental Biology **212**, 20, 3313–3329 (2009).

Yu, Y. and B. Tong, "A flow control mechanism in wing flapping with stroke asymmetry during insect forward flight", Acta Mechanica Sinica **21**, 3, 218–227 (2005).

Zbikowski, R., "Fly like a fly [micro-air vehicle]", Spectrum, IEEE **42**, 11, 46–51 (2005).

Zhang, Y.-L. and M. Sun, "Dynamic flight stability of hovering model insects: theory versus simulation using equations of motion coupled with navier–stokes equations", Acta Mechanica Sinica **26**, 4, 509–520 (2010).